On the relevance of tidal forcing in modelling the Mediterranean thermohaline circulation

G. Sannino , A. Carillo , G. Pisacane , C. Naranjo

A B S T R A C T

The four dominant constituents of the semi-diurnal and diurnal tides have been implemented in a regional eddy-resolving Mediterranean version of the Massachusetts Institute of Technology general circulation model to assess the role played by tides on the simulated Mediterranean thermohaline circulation. To this aim we have compared two 10-year hindcast simulations differing only for the inclu-sion/omission of tidal forcing. Following the recent recommendations suggested by Sannino et al. (2014) both simulations use the same model having a substantial increment of the horizontal resolution in the region of the Strait of Gibraltar. The results suggest that application of explicit tidal forcing in a Mediterranean model has non negligible effects on the simulated circulation in addition to the expected intensification of local mixing processes. The western basin exhibits an immediate response to the different characteristics of the inflowing AW observable in the modified deep water convection processes in the Gulf of Lion. The inclusion of tidal forcing also induces changes in the intermediate circulation of the Tyrrhenian Sea bringing to a better representation of local structures and a reinforcement of the global thermohaline cell. LIW dispersal paths in the eastern basin are also affected by tides.

1. Introduction

Compared to the adjacent Atlantic Ocean, the tidal signal in the Mediterranean Sea is relatively weak, on the order of 20–40 cm. Despite its being generally masked by atmosphere-induced and steric sea level variations, a more accurate determination of the Mediterranean tidal excursion has recently been urged, on one hand, by the need for verification of satellite altimeter measurements in the region and by sensitive geodetic applications (Vergos et al., 2002), on the other, by the vulnerability of coastal wetlands and lagoons to the combined effects of tide, circulation, surges and waves, coupled to freshwater discharge and sedi-ment transport in the proximity of river outlets (Janzen and Wong, 2002). A barotropic model of tide propagation in the Mediterranean Sea was set up by Tsimplis et al. (1995), and suc-cessfully used to investigate the relative magnitude of the internal Mediterranean equilibrium tide and of the Atlantic tidal wave entering the basin. Although the ability of the model to reproduce coastal and island gauge measurements might support the hypothesis that the baroclinic tidal component is of secondary importance in the Mediterranean basin, no definitive evidence was provided that tidal forcing should be negligible in the deeper layers, nor could such a modelling approach account for the role of residual currents in shallower areas. As a matter of fact, although many practical management purposes are effectively served by simply considering the linear superposition of tides and wind driven surges (e.g. high water events in the Lagoon of Venice, Bargagli et al., 2002), impact evaluation in complex and sensitive coastal areas calls for a modelling framework capable of simultaneously describing all the relevant processes, including the residual circulation originating from the interaction of the density field, river flow, and the non-linear rectification of the periodic tides (Maas and Zimmermann, 1989). From this perspective, although basin scale numerical models do not have the ambition of resolving the detailed circulation of coastal and transitional waters, their use as drivers for dedicated higher resolution models would recom-mend the inclusion of as many interacting mechanisms as possible. From the point of view of climate studies, the Mediterranean region and its hydrological cycle receive great interest from the scientific community, as the area has been recognized as an hot spot in recent IPCC reports (e.g. Parry et al., 2007). In particular, ocean modelling studies suggest that the Mediterranean thermohaline circulation (MTHC) could be weakened in conditions of global greenhouse warming (Somot et al., 2006; Thorpe and Bigg, 2000), an event which would undoubtedly affect regional cli-mate, possibly triggering global feedback processes. It has recently been shown that in the Strait of Gibraltar (SoG in the following) the

water exchange between the Mediterranean and the Atlantic ocean is significantly affected by tidal forcing, the westward barotropic tide having the effect of raising the interface between the inflowing and outflowing waters and of reducing its thickness, thus re-stratifying the water column and determining the characteristics of the Atlantic water entering the basin (García-Lafuente et al., 2013). The relevance of such effect has been highlighted in Adloff et al. (2015), where it has explicitly been acknowledged as the largest in determining the evolution of the Mediterranean water masses, even surpassing that of socio-economic scenarios, and therefore needs to be appropriately accounted for in numerical simulation of the MTHC. Nevertheless, tides and thermohaline circulation on climate time scales have so far been treated separately, mainly due to the insufficient computational resources of most climate research laboratories, which imposed the implementation of relatively coarse spatial resolution models whose associated time step was at least two orders of magnitude larger than that needed to account for the fast barotropic tidal signal. This work is the natural continuation of the first attempt by Sannino et al. (2009) to explicitly resolve the Strait dynamics in an eddy-permitting model over the entire Mediterranean basin, by means of a two-way local grid refinement.

We conduct a preliminary evaluation of the effects of tidal forcing on the simulated MTHC by comparing results from two hindcast numerical simulations, with and without tidal forcing, both implementing a high resolution representation of the SoG following the reccommendation suggested by Sannino et al. (2014). Such exploratory experiments only cover ten years, and our analy-sis is therefore restrained to the features that can be associated to the faster basin response on the simulated time scales, with the ambition of providing guidance for future research. The model and numerical experiments are described in Section 2. We first ver-ify that the representation of tide as to amplitude, phase, and resid-ual currents is realistic through comparison with previous works and observations (Section 3) and then proceed to the analysis of results separating the direct effects in the Strait of Gibraltar (Section 4.1) from the alteration induced in the basin interior, fol-lowing the eastward path of the inflowing Atlantic water (Section 4.2). Conclusions are drawn in Section 5.

2. Model description

The model used for the presented experiments is based on the MITgcm (Massachusetts Institute of Technology general circulation model) developed by Marshall et al. (1997a,b); which was adapted to the Mediterranean region. It is run in its hydrostatic, implicit free-surface, partial step topography version (Adcroft et al., 1997). The implicit non-linear free surface formulation follows Campin et al. (2004), while the rescaled vertical height (z^*) coordinate is that suggested by Adcroft and Campin (2004). The model domain extends over the entire Mediterranean Sea and part of the Atlantic Ocean, including the Gulf of Cadiz at its western boundary. Model bathymetry (Figs. 1 and 2) is the result of: a merging procedure that involved three different datasets; a bilin-ear interpolation on the model grid; and, finally, a hand-made check for isolated grid point, islands and narrow passages. The three datasets used are: the Digital Bathymetric Data Base-Variable Resolution (DBDB) at 1' resolution for the Mediterranean basin, DBDB-2 for the Atlantic box, and the very high resolution digitalized chart of Sanz et al. (1991) for the SoG. A non-uniform curvilinear orthogonal grid was adopted, achieving a maximum horizontal resolution of about $\frac{1}{200}^\circ \times \frac{1}{200}^\circ$ in the SoG, while smoothly degrading eastward down to a regular $\frac{1}{16}^\circ \times \frac{1}{16}^\circ$ grid spacing, for a total of 1530 $*$ 708 grid points (Fig. 3). In order to adequately resolve the dynamics of the different overlying water masses in the Mediterranean, 72 vertical unevenly spaced z-levels were prescribed, the layer thickness going from 3 m at the surface to 300 m at the sea bottom. Vertical eddy viscosity and diffusivity coefficients are computed in the MITgcm using the turbulence closure model developed by Bougeault and Lacarrere (1989) for the atmosphere and adapted for the oceanic case by Gaspar et al. (1990).

2.1. Numerical experiments

Both simulations were initialized with MEDATLAS-II (MEDAR Group, 2002) climatology data for August, when the stratification is expected to be more stable. At the western boundary, a 3D relaxation of salinity and temperature towards the climatological monthly Levitus data (Levitus, 1982) was applied, with the relaxation time varying from 3 days to 30 days over the first 30 grid points. Outside the Atlantic box the simulations were forced by prescribing surface wind stress and heat and fresh water fluxes for the period 1958–1967, the freshwater flux being the net bal-ance of evaporation, precipitation and river runoff. E–P–R was applied as a real fresh water flux in conjunction with the non-lin-ear free surface numerical scheme. Atmospheric fields were pro-vided by the ECMWF ERA40 reanalysis database (provided by the European Centre for Medium-Range Weather Forecasts), at a tem-poral resolution of six hours and a spatial resolution of about $1.125^\circ \times 1.125^\circ$, while the climatological river discharge was pre-scribed according to Struglia et al. (2004) for the main 68 catch-ments. The Black Sea net flow through the Dardanelles has been imposed following Stanev et al. (2000). A mild surface relaxation

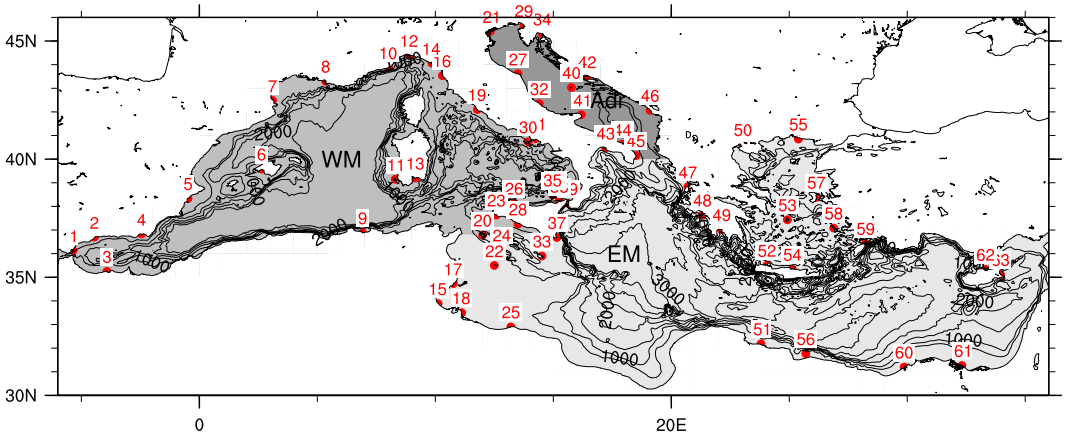

Fig. 1. Mediterranean model bathymetry. The isobaths every 500 m are indicated. The main three sub-basins, Western Mediterranean (WM), Adriatic Sea, and Eastern Mediterranean (EM) are shaded with different grey intensity. Numbers indicate the location of the tide gauges selected for comparison with the model.

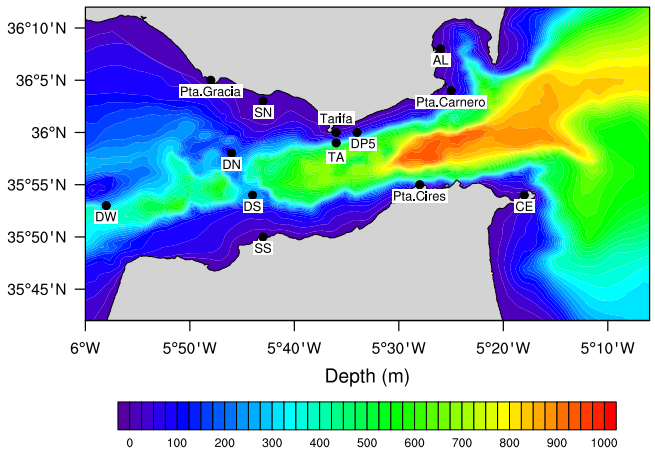

Fig. 2. Model bathymetry of the Strait of Gibraltar with the location of tide gauges.

to temperature and salinity climatological values was also applied, with relaxation times of 8 and 15 days respectively. A consistency check was performed on the resulting model surface fluxes, by verifying that their climatological means were in agreement with current estimates. The integral heat flux over the entire Mediterranean basin averaged over the ten years of the experiments was found to be -7.5 W m^{-2}, and the correspondent freshwater flux was 0.985 m/y, both values being within the accepted range (i.e. Macdonald et al., 1994).

The two experiments only differ by the inclusion (ExpT) or the omission (ExpNT) of tides. ExpT considers both internal equilibrium and lateral, propagating from the Atlantic Ocean, tides. The four main lunar, solar and luni-solar tidal components (M_2, O_1, S_2, K_1) have been prescribed. The diurnal and semi-diurnal equilibrium tide η_n^d and η_n^{sd} have been defined according to Kowalik and Proshutinsky (1994):

$$\eta_n^d = H_n^d sin2\phi cos(\sigma_n^d t + X_n^d + \lambda)$$

$$\eta_n^{sd} = H_n^{sd} cos^2\phi cos(\sigma_n^{sd} t + X_n^{sd} + 2\lambda)$$

where n denotes the nth constituent characterized by amplitude H_n, angular frequency σ_n, phase X_n. λ and ϕ correspond to longitude and latitude. It has been included throughout the domain as an additional body forcing term acting on the momentum equation. The lateral tidal component was applied as a western open boundary condition where the tidal values have been derived from the OTIS global inverse tide model (Egbert and Erofeeva, 2002). These values have been tuned until a reasonable agreement between the model prediction and the tide gauge data was achieved in the Mediterranean basin. Output fields were stored at 1 day temporal resolution over the whole basin interior. In order to achieve the necessary detailed description of the dynamics within the SoG, this resolution was increased to 3 h between 6.22°W and 5.33°W.

3. Validation of tidal forcing: comparison with data and previous modelling studies

In the Mediterranean Sea the tide is mainly semidiurnal exhibiting standing-wave regimes in four large areas separated by narrow nodal zones near Alicante, Tunis, and Crete. Shallow-sea resonances occur in the Northern Adriatic Sea and in the Gulf of Gabes, while the Adriatic also resonates to the otherwise weak

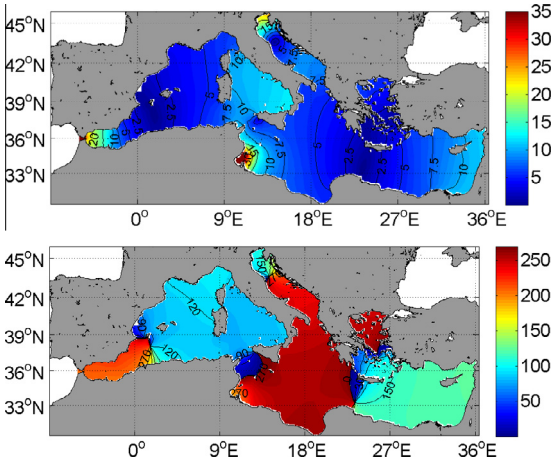

Fig. 4. M_2 constituent estimated by the barotropic sea surface height. Upper panel, amplitude in cm, lower panel, phase in degrees.

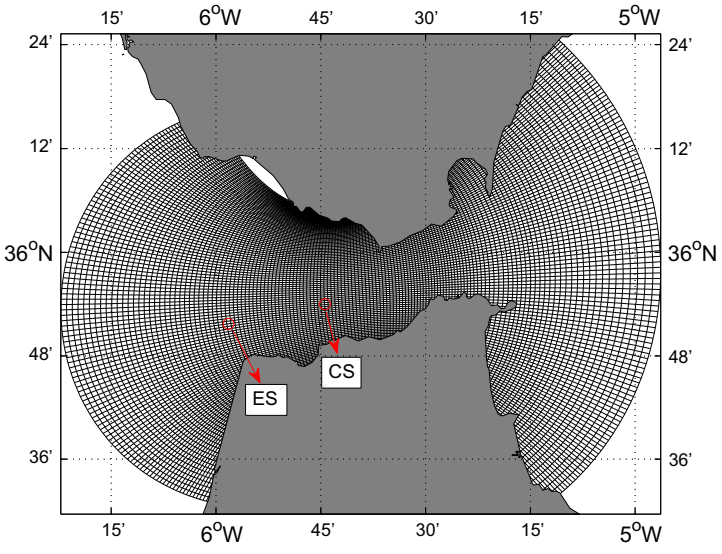

Fig. 3. Model grid in the Strait of Gibraltar. Espartell Sill (ES) and Camarinal Sill (CS) are marked on the map of the strait.

K_1 component (Defant, 1961). In Tsimplis et al. (1995), the incoming Atlantic tidal wave was shown to dominate up to 1°E, while further east its main effect is to modify the response to the equilibrium tide, notably by damping it by a factor of 0.5 in the Northern Aegean Sea, as already argued by Vincent and Canceill (1993), and by changing the location of the amphidromes.

Table 1
Observed (Obs) and Modeled (Mdl) Amplitudes (a_o, a_m) for the 63 Tide Gauges considered.

Tide Gauge	Location	Latitude	Longitude	M_2		S_2		O_1		K_1	
				Obs	Mdl	Obs	Mdl	Obs	Mdl	Obs	Mdl
1	Gibraltar	36°08′	05°21′W	29.8	29.2	10.7	12.9	0.9	1.8	2.0	1.6
2	Malaga	36°42′	04°27′W	18.0	18.1	7.0	8.2	2.0	1.3	3.0	2.5
3	B. Hoceima	35°15′	03°55′W	18.0	16.9	7.0	7.6	1.0	2.0	4.0	3.7
4	Almeria	36°50′	02°27′W	9.0	9.4	4.0	4.5	2.0	1.1	3.0	2.9
5	Alicante	38°20′	00°29′W	2.0	2.4	1.0	1.3	2.0	1.4	4.0	3.1
6	Palma	39°35′	02°38′E	3.0	3.2	1.0	1.3	2.0	2.0	4.0	3.1
7	Banyuls	42°29′	03°06′E	4.6	4.4	1.8	2.1	1.9	2.2	3.2	3.1
8	Marseille	43°18′	05°21′E	7.0	6.0	2.0	2.4	2.0	2.6	3.0	3.0
9	Skikda	36°53′	06°55′E	5.6	6.0	2.2	2.4	2.0	3.1	2.3	2.1
10	Porto Maurizio	43°52′	08°01′E	8.3	8.2	3.4	3.0	1.6	3.3	3.6	3.0
11	Carloforte	39°09′	08°18′E	6.5	5.9	2.6	2.7	1.9	3.2	3.2	3.1
12	Genova	44°24′	08°54′E	8.6	8.5	3.2	3.2	1.4	3.6	3.3	3.0
13	Cagliari	39°12′	09°10′E	7.6	8.3	2.8	3.7	1.8	2.9	3.2	2.7
14	La Spezia	44°04′	09°51′E	9.4	8.8	3.4	3.4	1.4	3.8	3.7	3.0
15	Gabes	33°53′	10°07′E	51.1	50.1	36.4	31.1	0.5	3.4	2.5	2.1
16	Livorno	43°32′	10°18′E	8.5	7.1	3.4	3.6	1.8	3.8	4.0	3.6
17	Sfax	34°44′	10°46′E	41.6	40.6	26.7	25.0	0.8	0.5	1.8	1.4
18	Zarzis	33°30′	11°07′E	21.9	20.6	15.3	10.5	0.9	0.7	2.0	2.0
19	Civitavecchia	42°06′	11°47′E	10.9	10.5	4.1	5.1	1.2	3.3	2.7	2.5
20	Pantelleria	36°47′	12°00′E	1.6	1.0	1.9	1.7	1.4	1.1	2.0	1.5
21	Venice	45°25′	12°20′E	23.4	22.1	14.1	14.1	5.6	5.3	17.9	16.4
22	Lampedusa	35°30′	12°30′E	6.6	6.5	4.2	4.9	0.7	0.8	0.9	0.2
23	Mazara del Vallo	37°38′	12°35′E	4.3	2.3	1.8	1.8	1.6	1.4	3.5	3.1
24	SG	36°10′	12°49′E	4.8	4.0	3.1	3.5	0.9	0.8	0.5	0.5
25	Tripoli	32°54′	13°12′E	11.1	12.5	5.4	4.5	0.6	0.3	2.0	0.9
26	Palermo	38°08′	13°20′E	10.6	11.5	4.1	5.4	1.2	1.1	3.2	2.6
27	Ancona	43°37′	13°30′E	6.6	6.8	3.6	3.7	4.2	3.6	13.0	6.6
28	P. Empedocle	37°15′	13°30′E	4.5	4.2	3.2	3.3	1.4	1.4	1.8	1.4
29	Trieste	45°39′	13°45′E	26.3	26.0	15.2	16.6	6.1	6.0	19.7	8.5
30	Ischia	40°44′	13°56′E	12.0	11.3	5.0	5.4	1.0	0.9	3.0	2.5
31	Napoli	40°52′	14°16′E	11.1	11.5	4.4	5.5	1.0	4.0	2.8	2.5
32	Ortona	42°21′	14°24′E	6.4	6.3	4.5	4.5	3.4	3.7	9.7	9.7
33	Malta	35°54′	14°31′E	6.0	8.7	4.0	3.7	1.0	1.7	1.0	0.6
34	Bakar	45°18′	14°32′E	10.6	13.8	5.5	8.2	4.1	4.2	13.8	13.3
35	Lipari	38°29′	14°58′E	12.0	12.0	4.5	5.7	1.1	1.1	3.1	2.9
36	Catania	38°30′	15°06′E	6.4	6.1	3.4	5.7	1.1	1.1	1.5	1.3
37	Capo Passero	36°41′	15°09′E	6.7	7.2	3.5	3.8	0.9	0.4	1.9	1.6
38	Milazzo	38°13′	15°15′E	12.0	12.2	4.7	5.8	1.1	1.2	3.3	2.9
39	Reggio Calabria	38°07′	15°39′E	6.2	6.6	3.1	3.5	0.9	0.8	1.3	1.5
40	Santadrea Island	43°02′	15°46′E	6.8	5.9	4.4	4.4	2.5	2.2	6.8	6.3
41	Vieste	41°53′	16°11′E	7.9	8.8	5.1	5.9	1.5	1.9	4.2	3.9
42	Split	43°30′	16°26′E	8.0	7.6	5.6	4.8	2.7	2.1	8.8	8.3
43	Taranto	40°28′	17°13′E	6.5	6.3	3.7	3.5	0.8	0.5	1.8	1.5
44	Brindisi	40°38′	17°56′E	8.7	8.7	5.2	5.6	1.5	1.3	4.6	3.6
45	Otranto	40°09′	18°30′E	7.0	6.8	4.0	4.1	1.0	0.9	2.3	1.7
46	Bar	42°04′	19°06′E	9.2	8.8	5.6	5.8	1.4	1.1	4.8	4.7
47	Lefkas	38°50′	20°42′E	4.0	4.8	2.2	2.7	0.6	0.6	1.4	1.1
48	Katakolo	37°38′	21°19′E	3.3	3.9	1.6	2.0	0.5	0.9	1.3	1.0
49	Kalamata	37°01′	22°08′E	2.2	2.8	1.1	1.7	0.5	0.6	1.2	1.0
50	Thessaloniki	40°37′	23°02′E	9.0	9.5	6.1	5.6	1.3	0.9	2.6	2.4
51	Tobruch	32°11′	23°48′E	1.4	2.4	1.3	1.0	0.5	0.2	0.6	0.6
52	Souda	35°30′	24°03′E	1.0	1.5	0.8	0.7	0.6	0.5	1.4	1.0
53	Syros	37°26′	24°55′E	2.0	1.9	1.0	0.4	1.0	0.8	1.9	1.3
54	Iraklion	35°20′	25°08′E	1.5	2.5	1.1	1.1	0.9	0.8	1.8	1.4
55	Alexandroupolis	40°51′	25°23′E	7.1	8.2	5.0	3.1	1.3	1.3	0.3	0.3
56	Portobardia	31°46′	25°42′E	2.9	2.0	2.9	2.2	0.8	0.7	1.2	0.9
57	Chios	38°23′	26°09′E	4.4	4.5	2.9	0.7	1.3	1.5	2.3	1.9
58	Leros	37°05′	26°53′E	2.1	2.7	1.3	1.2	1.1	1.0	2.0	1.9
59	Rodos	36°26′	28°14′E	4.4	4.1	2.7	3.1	1.1	1.0	1.8	1.3
60	Alexandria	31°12′	29°52′E	7.2	8.5	4.1	3.8	1.3	1.1	1.7	1.0
61	Port Said	31°16′	32°19′E	11.2	12.9	6.9	5.9	1.7	1.7	2.1	1.6
62	Kyrenia	35°20′	33°19′E	10.1	11.1	6.4	5.0	1.8	1.3	2.4	1.6
63	Famagusta	35°07′	33°57′E	11.0	12.2	7.3	6.5	1.8	1.5	2.1	1.7

Table 2
Comparison between observed and predicted amplitudes A and Phases P of M_2 and S_2 tidal elevations.

Location	Latitude	Longitude	Observed M_2		Predicted M_2		Observed S_2		Predicted S_2	
			A (cm)	P (deg)	A (cm)	P (deg)	A (cm)	P (deg)	A (cm)	P (deg)
García-Lafuente (1986)										
Pta. Gracia	36°05.4′	05°48.6′W	64.9 ± 0.2	49.0 ± 0.5	67.5	40.4	22.3	74.0	29.3	69.7
Tarifa	36°00.2′	05°36.4′W	41.5 ± 0.2	57.0 ± 0.5	40.9	39.0	14.2	85.0	18.3	68.6
Pta. Cires	35°54.7′	05°28.8′W	36.4 ± 0.2	46.5 ± 0.5	34.5	46.5	14.1	74.0	15.3	74.0
Pta. Carnero	36°04.3′	05°25.7′W	31.1 ± 0.2	47.5 ± 0.5	29.9	37.1	11.5	71.0	13.6	67.2
Candela et al. (1990)										
DN	35°58′	05°46′W	60.1	51.8	58.1	43.3	22.5	73.8	25.3	71.9
DS	35°54′	05°44′W	54.0	61.8	55.1	46.8	21.1	83.3	23.9	74.5
SN	36°03′	05°43′W	52.3	47.6	51.7	37.2	18.5	73.4	22.8	67.5
SS	35°50′	05°43′W	57.1	66.8	55.0	52.3	20.6	92.3	23.5	78.9
DW	35°53′	05°58′W	78.5	56.1	73.1	47.3	29.0	82.2	31.2	74.9
TA	36°01′	05°36′W	41.2	41.2	40.9	39.0	14.7	67.9	18.3	68.6
AL	36°08′	05°26′W	31.0	48.0	28.3	37.6	11.1	73.9	12.9	67.7
CE	35°53′	05°18′W	29.7	50.3	27.6	48.7	11.4	75.6	12.3	76.1
DP5	36°00′	05°34′W	44.4	47.6	40.4	39.6	16.1	73.9	18.0	69.0

3.1. Tidal amplitude and phase

The reliability of the modelled tides was checked in a preliminary barotropic experiment in which only the internal and equilibrium tidal forcing was prescribed. We performed the harmonic analysis of the simulated sea surface height over the entire Mediterranean basin, following Foreman (1977), by using the software package developed by Pawlowicz et al. (2002). Fig. 4 shows the computed amplitude and the phase of the M_2 tidal component (panel a and b, respectively). The locations where modelled values could be compared to tidal gauge observations (derived from Tsimplis et al., 1995), basically confirming previous results, are shown in Fig. 1. The combined effect of lateral and equilibrium tides, locally enhanced by resonance phenomena, gives rise to values higher than 10 cm near the Strait of Gibraltar, in the northern Adriatic Sea, in the Gulf of Gabes and in the easternmost part of the basin, while the tide-induced sea level variation remains below such threshold in the rest of the basin. The four amphidromic points already described by Tsimplis et al. (1995) are found south of the Balearic islands, in the Sicily Channel (although somewhat dislocated towards the North-East), in the northern Adriatic and between the northern coast of Africa and Crete. The comparison of the principal semidiurnal (M_2, S_2) and diurnal constituents (K_1, O_1) to observations is presented in Table 1. The modelled M_2 and S_2 amplitudes show good agreement with those measured at the available tide gauges in the whole Mediterranean Sea. The O_1 component exhibits the highest relative errors, with amplitudes twice the observed in some western locations. The model fails to represent the large tidal range (up to 2 m) in the Gulf of Gabes, unusual for the Mediterranean basin and attributable to a phenomenon of semidiurnal resonance (Sammari et al., 2006). This is probably due to the small scale characteristics of local topography, which cannot be captured at the resolution adopted for the present experiments.

On the contrary, due to the enhanced local resolution, reasonable agreement is found in the SoG region, as shown in Table 2. The table reports the observed and simulated amplitudes (A) and phases (P) for the two principal semidiurnal tidal components, representing more than 80% of the total tidal signal (Candela et al., 1990). Amplitudes are found to differ by no more than 5 cm for M_2 and 7 cm for S_2, while deviations in phase amount to 18° for M_2 and 16° for S_2.

3.2. Tidal rectification and residual currents

The basic mechanism of tidal rectification over complex bathymetry consists of a non-linear momentum transfer from the oscillating tidal currents to the mean flow. Such process can

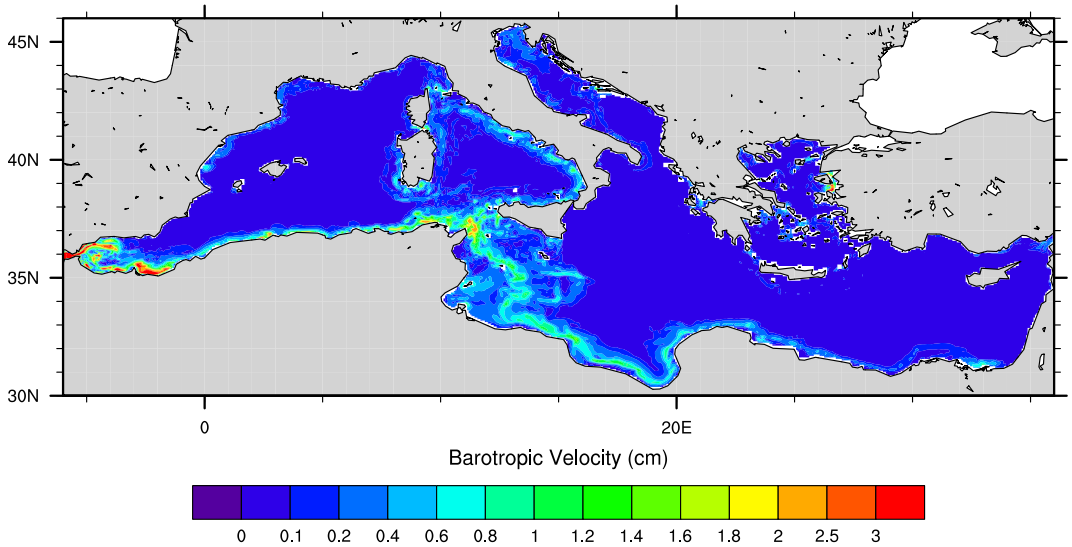

Fig. 5. Difference between ExpT and ExpNT barotropic velocity time-averaged over the first 30 days of the simulation.

alternatively be interpreted as a net cross-isobath advection of relative tidal vorticity, resulting from the difference between the negative vorticity advected by the flood tidal current to shallow regions, and the positive vorticity advected by the ebb tidal current to deep regions, which can maintain the along isobaths residual current against friction over a tidal cycle (Zimmerman, 1981; Maas and Zimmerman, 1981). The induced rectified flow crucially depends on the typical scales of bottom topography, on the magnitude of the tidal current, on friction and stratification, increasing in magnitude as bathymetry becomes steeper and tidal currents more intense, while friction and stratification both enhance turbulent mixing and trigger complex feedbacks (Loder, 1980; Tee, 1985; Loder and Wright, 1985; Maas and Zimmerman, 1989a,b). For the first time, Chen and Beardsley (1995) attempted to fully describe such non-linear interactions by using a 3D numerical model with idealized topography, both in homogeneous conditions and with prescribed initial stratification. They observed that the stratification induced internal tidal waves, giving rise to horizontal tidal mixing and enhancing the cross-isobath momentum transfer. Subsequent studies mainly focused on relatively shallow coastal areas of the global ocean where tidal currents are more intense.

In the Mediterranean basin, due to the limited amplitude of tides, a comprehensive study of the insurgence and relevance of tidal residual currents is still lacking, with the exception for a few studies dedicated to the Adriatic sub-basin (Cushman-Roisin and Naimie, 2002), which exhibits both the shallowness and tide excursion necessary to expect a non-negligible effect. However, such requirements are also met by the Sicily Channel, whose complex surface dynamics controls the propagation of the AW into the Eastern Basin but is still largely unknown (Millot and Taupier-Letage, 2005). The residual current field in the sea being defined as the mean velocity field over a time sufficiently long to cancel transitory wind currents and tidal oscillations, we computed the tidal contribution as the difference between the barotropic velocity fields from ExpT and ExpNT, averaged over the first month of the simulation (Fig. 5). The use of vertical means was dictated by the necessity of comparing our results to those obtained by Cushman-Roisin and Naimie (2002) with their barotropic model, while limiting the analysis to the initial month ensures the exclu-sion of effects arising from the long term evolution of the cir-culation. Despite the lower spatial resolution, our results agree with those of Cushman-Roisin and Naimie (2002), with maximum currents of about 1 cm/s along the coast of Croatia. In the Sicily Channel a significant stream is observed, with velocities of about

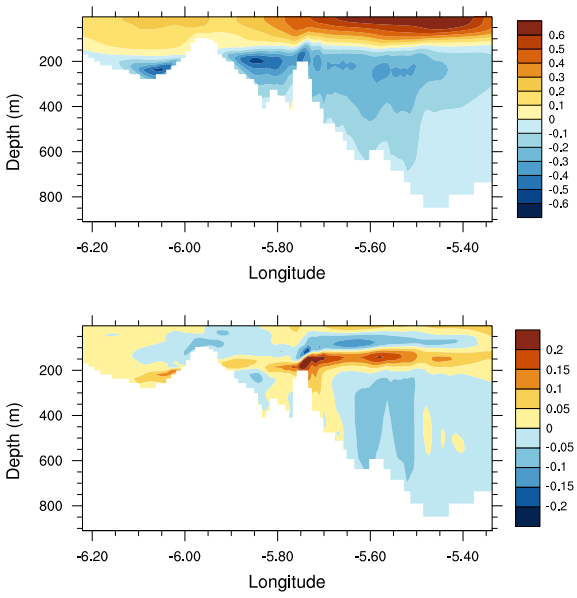

Fig. 7. Zonal velocity along-strait section. Upper panel ExpT simulation, lower panel difference between ExpT and ExpNT simulations. Time-average over the entire simulation period.

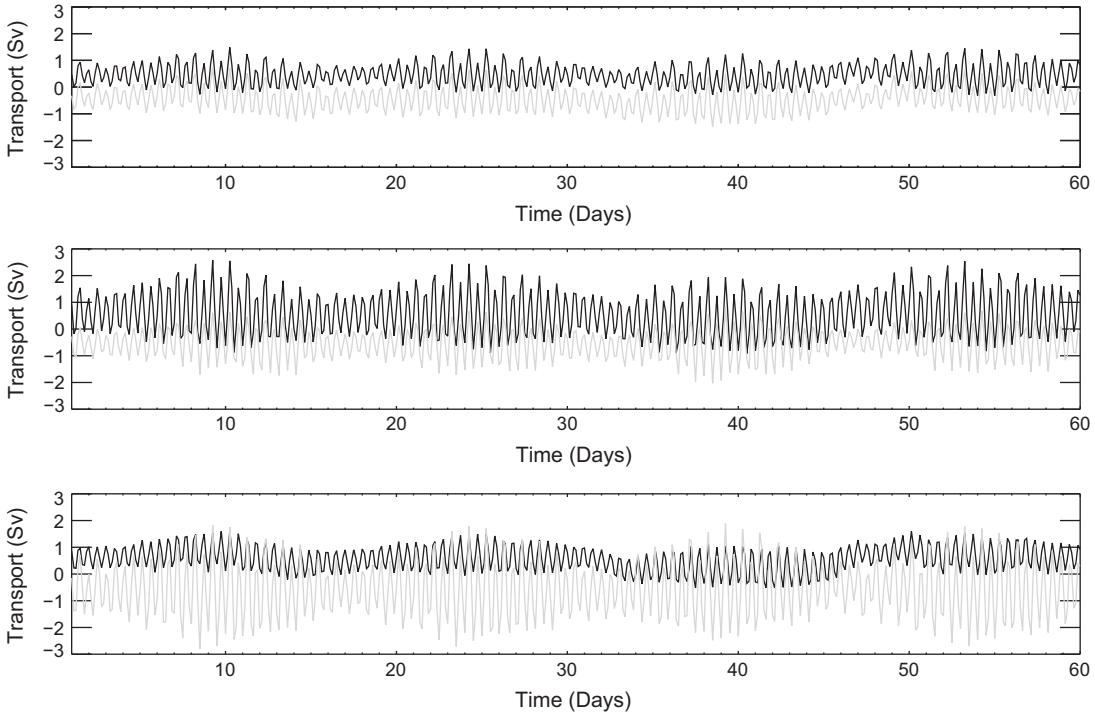

Fig. 6. Atlantic (black) and Mediterranean (grey) transports computed from ExpT simulation for sections at 6.22°W (upper panel), 5.76°W (middle panel) and 5.33°W (lower panel). Positive for eastward direction.

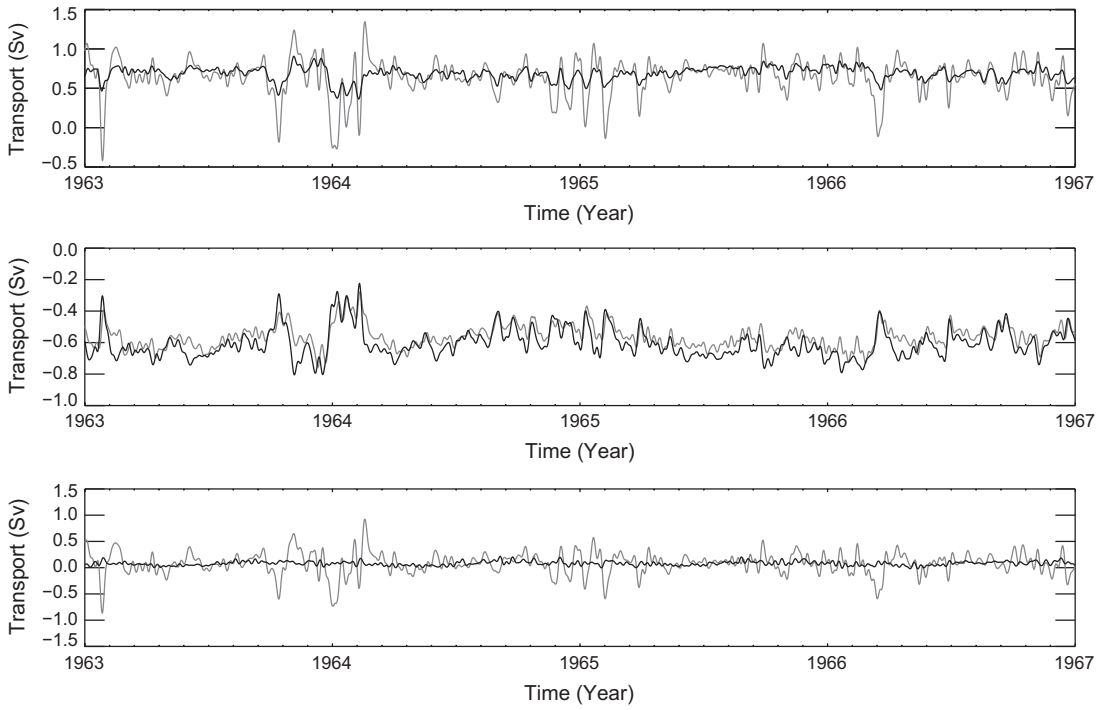

Fig. 8. Atlantic (upper panel), Mediterranean (middle panel) and net (lower panel) water transports at section 5.33°W for ExpT (grey line) and ExpNT (black line) simulations. Data have been filtered off periods less than 8 days.

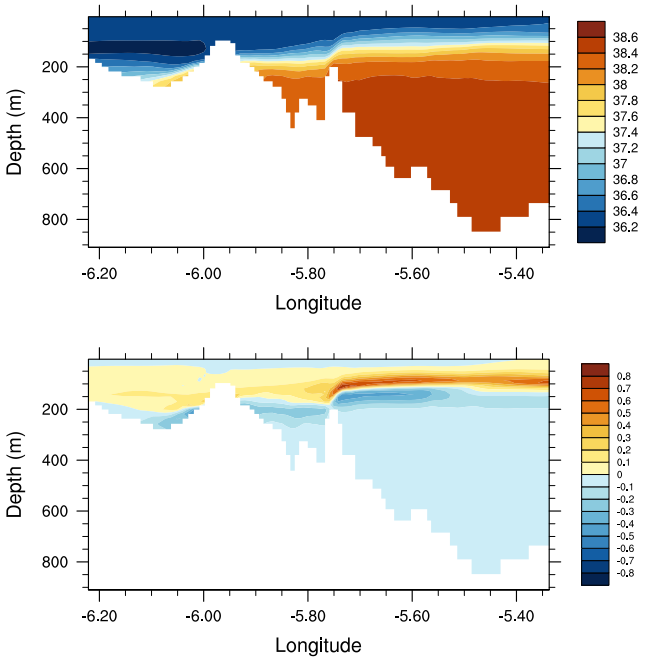

Fig. 9. Salinity along-strait section. Upper panel ExpT, lower panel difference ExpT-ExpNT. Time-average over the entire simulated period.

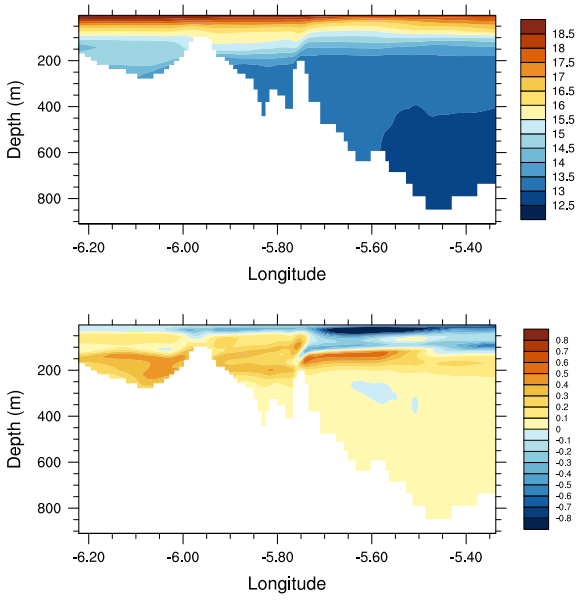

Fig. 10. Temperature along-strait section. Upper panel ExpT, lower panel difference ExpT-ExpNT. Time-averaged over the entire simulated period.

$1 \div 2$ cm/s, which, however, represent a small percentage of the average velocity in the area, which can be as large as 50 cm. A more detectable signal might have been expected in the Gulf of Gabes and along the coast of Tunisia, due to the large tidal range combined to extreme shallowness in this area. However, as already noted, the model used in this study fails to adequately represent local tides, and consequently also misses their second order effects.

4. Results: effects of tidal forcing on the modelled circulation of the Mediterranean Sea.

4.1. Two-way exchange and tide-induced mixing in the Strait of Gibraltar

The MITgcm has already been effectively employed in 3D simulations of the Mediterranean circulation (Sannino et al., 2009; Carillo et al., 2012; Fenoglio-Marc et al., 2013), and the SoG dynamics with tidal forcing, both as a support to hydraulic analysis

and in a model inter-comparison study (Sanchez-Garrido et al., 2011; Sannino et al., 2014). The results presented here confirm its reliability in representing the observed exchange flows in a longer simulation extended to the whole Mediterranean basin.

The two-way water exchange through the Strait of Gibraltar consists of a strong surface current of relatively fresher and warmer water from the ocean (AW) and a deep-water current of saltier and colder Mediterranean Water (MW), outflowing into the ocean and sinking in the North Atlantic in the form of a gravity current. The water exchange regime within the Strait critically depends on the number and location of its hydraulic controls, being submaximal if subject to only one control in the western part, or maximal if the flow is also controlled in the eastern part, with different implications for the characteristics of the circulation. Local dynamics are strongly influenced by tides, which are responsible for the amplitude modulation of water transport and for the substantial vertical mixing that has been observed (García-Lafuente et al., 2013), as well as for the migration of the eastern hydraulic control (Armi and Farmer, 1988 and Farmer and Armi, 1988). As a matter of fact, in addition to a barotropic tidal wave, tidal forcing also generates internal baroclinic waves due to the interactions between the vertical discontinuities in water properties, the intense tidal currents and the steep local topography. In particular, a hydraulic jump occurring west of the Camarinal Sill drains energy from the mean flow until the eastward acceleration of the tidal current induces a subcritical regime over the sill, and an eastward bore is released, which subsequently breaks into a packet of solitary internal waves (Sanchez-Garrido et al., 2011). The propagation of the internal bore causes the interface between the two water layers to oscillate violently and turbulent mixing to occur. Although the presence of a thick interfacial layer generated by vertical entrainment and mixing limits the applicability of a two-layer description of the flow regime in the strait (Bray et al., 1995; Sannino et al., 2009), the following diagnostics is based on such a simplified model, where, however, the frequent ambiguity in defining the interface between Mediterranean and Atlantic waters was at least removed. We defined the interface as the tropical month-averaged salinity surface corresponding to the zero tropical month-averaged velocity field, approximately locating it in the middle of the layer in which entrainment and mixing occur between Mediterranean and Atlantic waters. Indeed, the tidal signal in the strait is so strong as to reverse the inflow or the outflow during part of the tidal cycle,

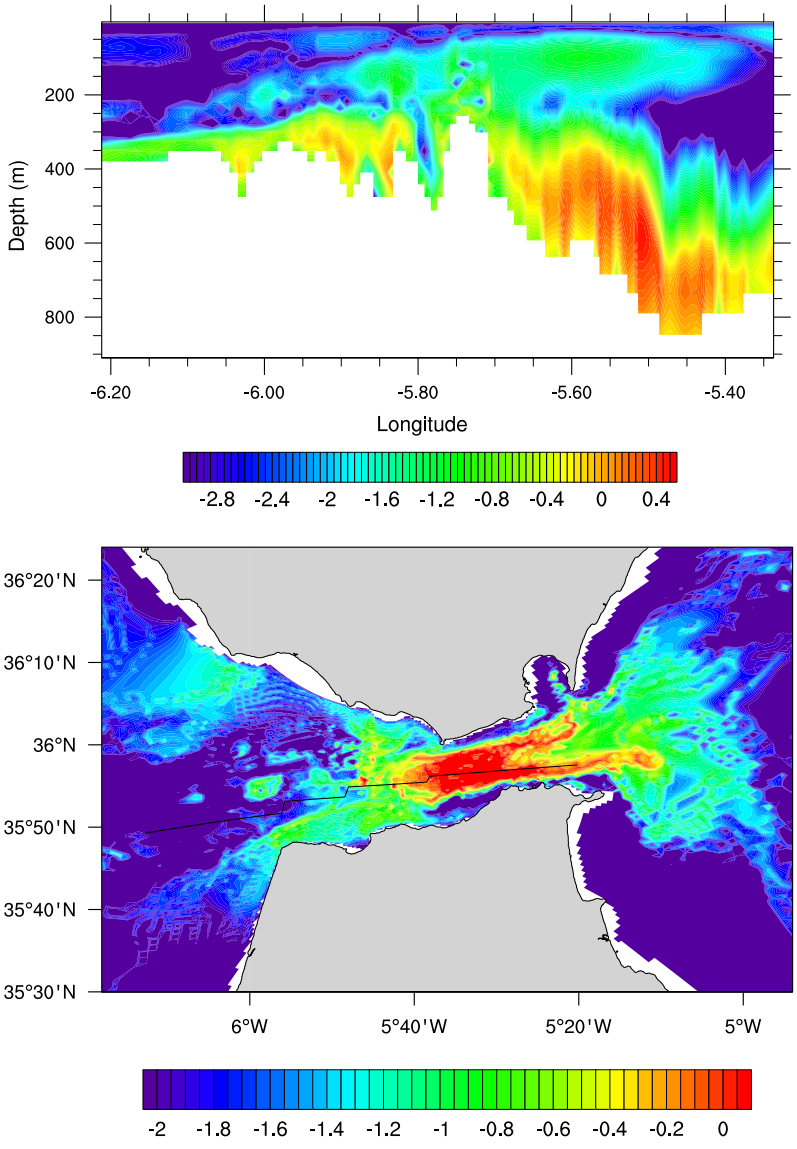

Fig. 11. Absolute difference in the SoG between the vertical mixing in ExpT and ExpNT. The position of the section in the upper panel is shown by the black line in the lower panel. Lower panel map shows the maximum computed over the entire depth. Values are time-averaged over the last year of the simulation. Logarithmic values are shown.

so that the surface of zero velocity usually identified as the interface is not always recognizable. Moreover, the underlying assumption that the transition layer is stagnant and the Atlantic and the Mediterranean layers are decoupled must clearly be abandoned in view of the already mentioned recent literature.

Fig. 6 shows the time series of transports in the upper and lower layers from ExpT, for three cross sections along the strait, located at 6.22°W, 5.76°W and 5.33°W and corresponding to the western end, Camarinal Sill (CS) and the eastern end, respectively. For the sake of readability, the time axis only covers 60 days, which are representative of the cyclic behaviour of transports along the whole ten year simulation. Results are in qualitative agreement with both experimental data (Candela et al., 1990) and previous numerical findings (Sannino et al., 2004), showing the periodical reversal of the westward transport in the lower Mediterranean layer, both at the Camarinal Sill and at the easternmost section, as well as its amplitude modulation by the tidal signal. At the west-ernmost section, the evident modulation is somewhat lost, but a clear periodic inversion is still visible. Conversely, the eastward transport in the upper Atlantic layer, similarly modulated by tide at the two westernmost locations, experiences intermittent and less significant reversals, with the notable exception of the CS time series, where it exhibits a cyclic inversion analogous to that of the lower layer. Still at the sill, both signals have comparably large amplitudes. At the easternmost section, the periodic behaviour of upper layer appears to have a less definite frequency spectrum, as a specular analogue of the Mediterranean outflow time series at its Atlantic outlet, and to have transferred part of its function to the underlying layer. In other words, it is possible to follow the propagation of the Atlantic tidal wave, reaching its maximum amplitude in correspondence of the CS, and then loosing coherence and momentum to the benefit of the underlying Mediterranean layer at the easternmost section, as a result of the baroclinic processes occurring within the strait. A similar picture could be given for the Mediterranean outflow, provided the propagation axis was reversed. A more appropriate description should account for the

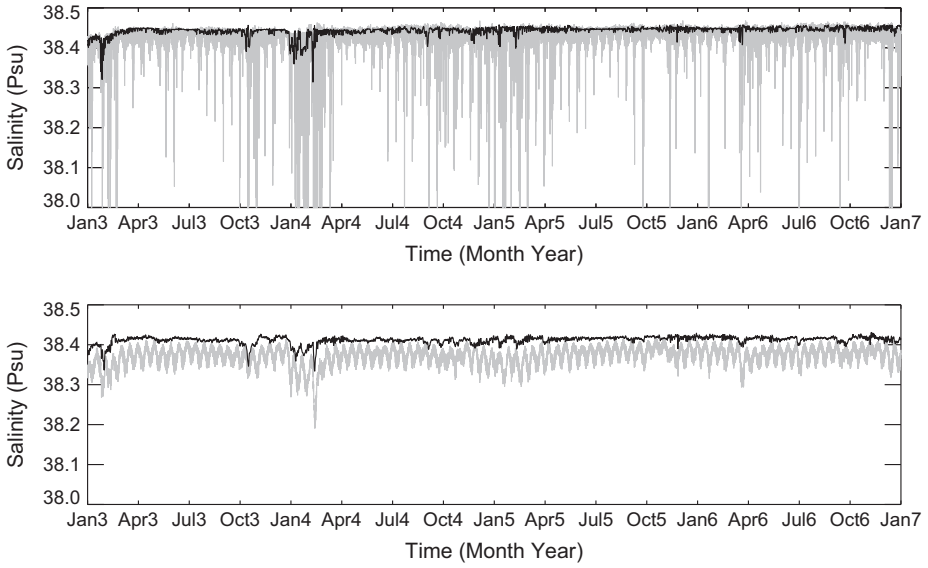

Fig. 12. Time series of salinity vertical maximum for the years 1963–1967. Upper panel for the CS and lower panel for ES. ExpT in grey, ExpNT in black.

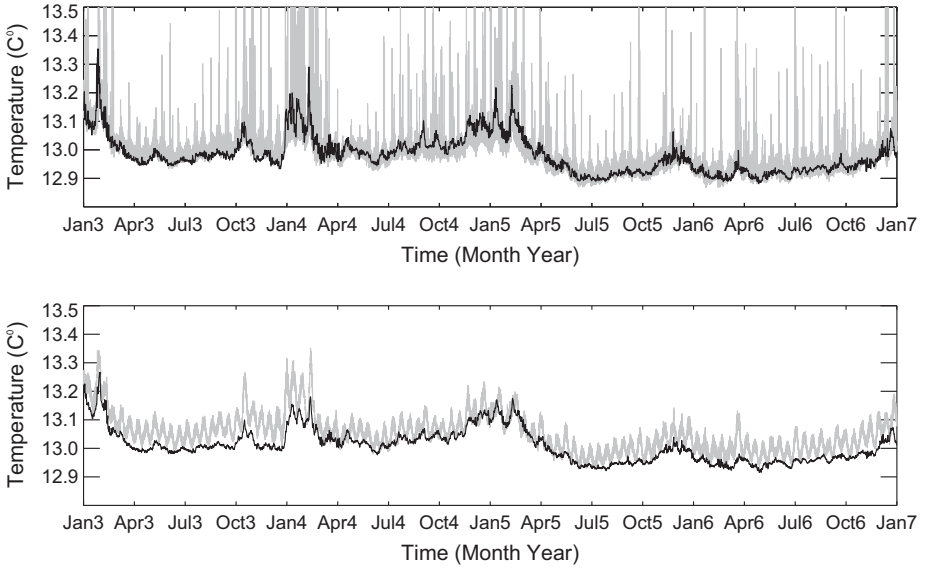

Fig. 13. Time series of the vertical minimum of temperature for the years 1963–1967. Upper panel for the CS and lower panel for ES. ExpT in grey, ExpNT in black.

formation of a proper interface layer due to the entrainment and mixing of the two distinct waters within the strait, which is in fact itself responsible for the transport of mixed Atlantic-Mediterranean water alternatively in both directions everywhere along the strait, of magnitude comparable to that of both the Atlantic and Mediterranean layers (Sannino et al., 2009). Again we stress that the two-layer model is only adopted here as a plausible, although limited, diagnostic description, while the complex strait dynamics are fully represented and the resulting characteristics of the inflowing AW, which constitute the main objective of this study, are realistically simulated. In order to highlight the impact of tidal forcing on the numerical representation of the flow

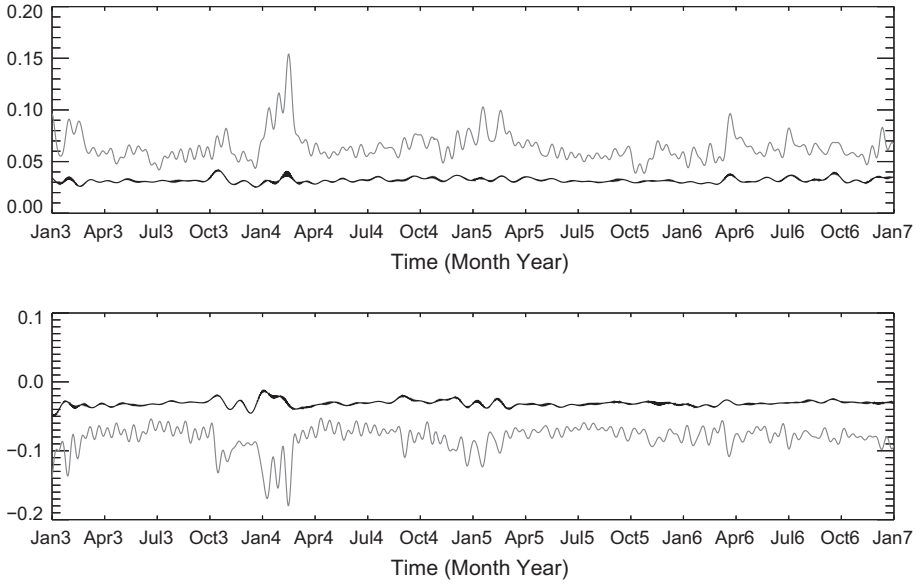

Fig. 14. Time series of the difference in CS and in ES between daily maximum salinity (upper panel) and daily minimum temperature (lower panel). Data are filtered off frequencies higher than 30 days. ExpT in grey, ExpNT in black.

Table 3
3D averaged temperature (T in °C) for the ExpT and ExpNT experiments averaged over the entire period (1958–1967). MEDATLAS database (OBS) has been averaged over the same period.

		$\langle T \rangle$	$\langle 0-100T \rangle$	$\langle 100-600T \rangle$	$\langle 600-bottomT \rangle$
	OBS	13.68	17.15	14.19	13.27
Med	ExpT	13.73 ± 0.03	16.83 ± 0.20	14.08 ± 0.12	13.35 ± 0.05
	ExpNT	13.73 ± 0.02	16.86 ± 0.20	14.09 ± 0.11	13.34 ± 0.05
	OBS	13.18	15.92	13.45	12.91
WM	ExpT	13.18 ± 0.05	15.86 ± 0.22	13.38 ± 0.12	12.88 ± 0.01
	ExpNT	13.18 ± 0.04	15.88 ± 0.22	13.38 ± 0.12	12.88 ± 0.01
	OBS	14.00	18.07	14.67	13.50
EM	ExpT	14.08 ± 0.03	17.49 ± 0.23	14.51 ± 0.12	13.63 ± 0.09
	ExpNT	14.08 ± 0.03	17.52 ± 0.21	14.52 ± 0.11	13.62 ± 0.08
	OBS	13.95	15.22	13.66	13.28
Adr	ExpT	13.86 ± 0.09	15.18 ± 0.14	13.51 ± 0.09	13.12 ± 0.09
	ExpNT	13.79 ± 0.11	15.12 ± 0.16	13.45 ± 0.09	13.04 ± 0.14

Table 4
3D averaged salinity (S in psu) for ExpT and ExpNT experiments averaged over the entire period (1958–1967). MEDATLAS database (OBS) has been averaged over the same period.

		$\langle S \rangle$	$\langle 0-100S \rangle$	$\langle 100-600S \rangle$	$\langle 600-bottomS \rangle$
	OBS	38.62	38.27	38.67	38.63
Med	ExpT	38.66 ± 0.02	38.55 ± 0.07	38.72 ± 0.02	38.66 ± 0.02
	ExpNT	38.66 ± 0.02	38.53 ± 0.06	38.72 ± 0.03	38.65 ± 0.02
	OBS	38.42	37.76	38.43	38.46
WM	ExpT	38.41 ± 0.01	37.96 ± 0.05	38.43 ± 0.01	38.45 ± 0.01
	ExpNT	38.41 ± 0.01	37.90 ± 0.05	38.43 ± 0.01	38.45 ± 0.01
	OBS	38.75	38.58	38.84	38.73
EM	ExpT	38.81 ± 0.04	38.88 ± 0.08	38.89 ± 0.04	38.77 ± 0.04
	ExpNT	38.80 ± 0.03	38.87 ± 0.08	38.89 ± 0.04	38.77 ± 0.03
	OBS	38.61	38.43	38.68	38.67
Adr	ExpT	38.76 ± 0.11	38.75 ± 0.13	38.77 ± 0.09	38.76 ± 0.12
	ExpNT	38.74 ± 0.09	38.72 ± 0.11	38.74 ± 0.08	38.74 ± 0.09

at the eastern inlet of the strait, Fig. 7 compares the climatological (i.e. averaged over the entire simulation period) along-strait velocity components in ExpT and ExpNT. East of CS, the average westward velocity of the outflowing Mediterranean layer is lower in ExpT than in ExpNT, and the eastward inflow velocity is accordingly reduced, coherently with the foregoing two-layer description. The time variability of the associated transports is reported in Fig. 8. It shows the Atlantic (upper panel) and Mediterranean (intermediate panel) water transports at 5.33°W, for ExpT (grey curve) and ExpNT (black curve), over the last four simulated years, for the sake of readability. Time scales of less than 8 days have been filtered out. Although exhibiting a general tendency to reduce negative anomalies, the outward transport of Mediterranean water does not change significantly between the two experiments, being

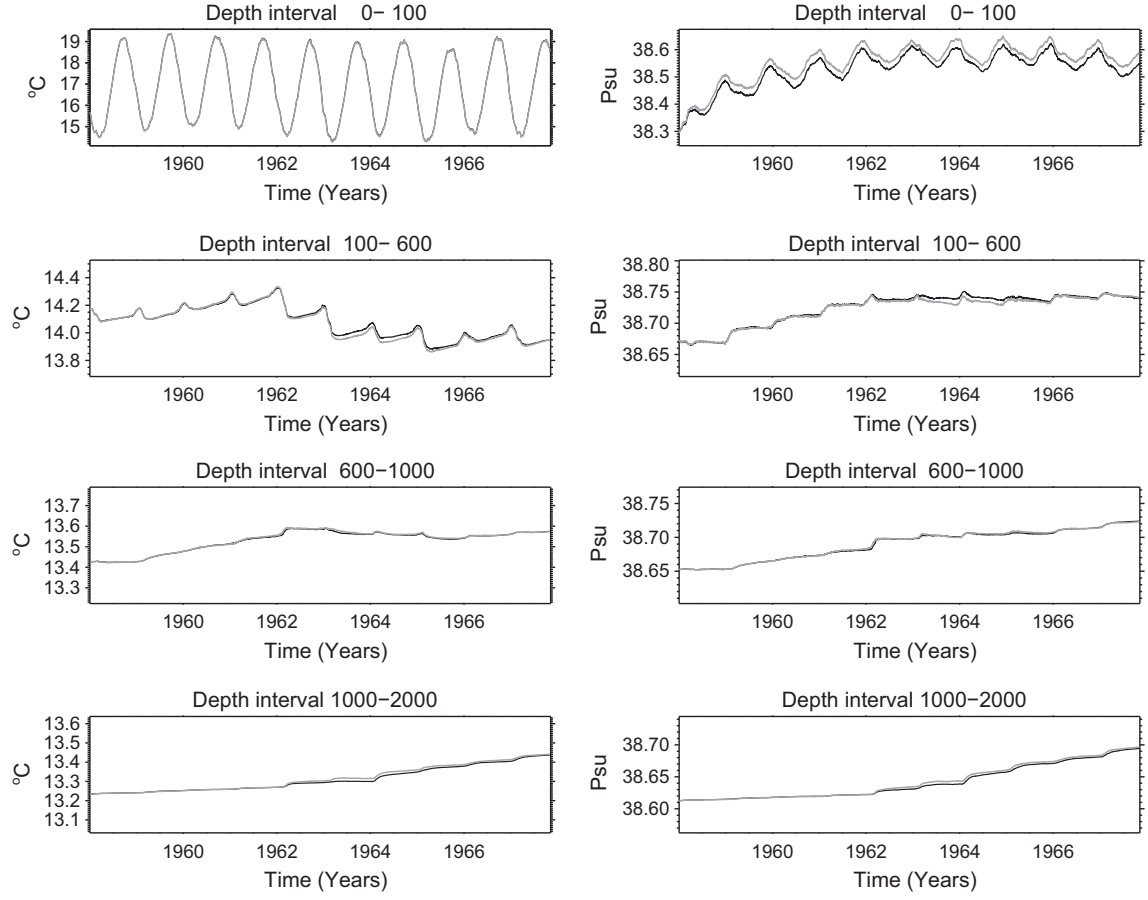

Fig. 15. Temperature (left panel) and salinity (right panels) averaged over the entire Mediterranean basin and different depth intervals. ExpT black line, ExpNT grey line.

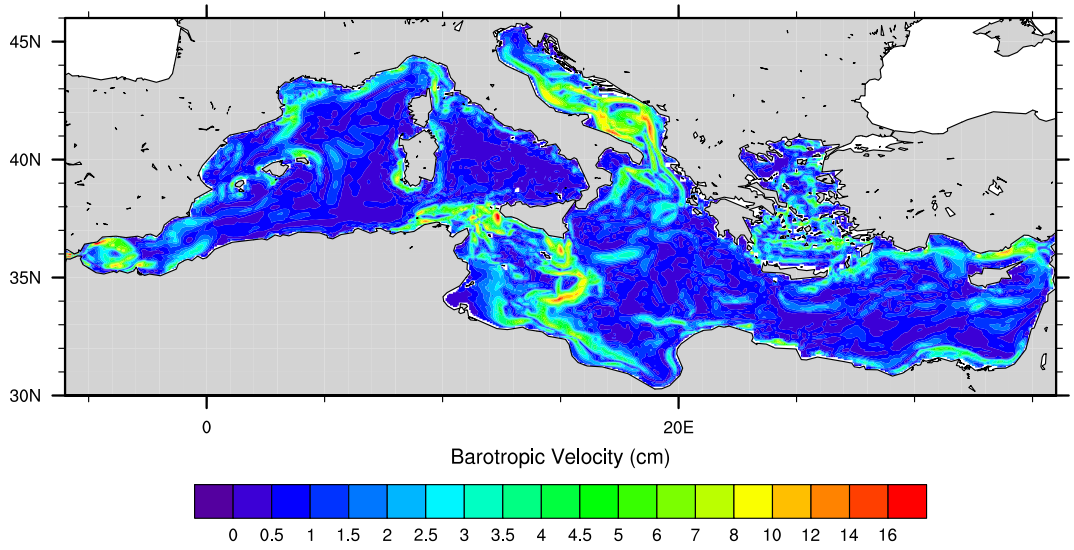

Fig. 16. Barotropic velocity time-averaged over the entire simulation for ExpT.

characterized by comparable inter-annual and high frequency variability, whereas tidal forcing evidently excites high frequency (∼14 days period) oscillations in the inward Atlantic transport, of amplitude often larger than twice the average value of 0.64 Sv, in particular during winter and spring.

In ExpT, the resulting net transport obviously retains the features of such tide-induced variability, exhibiting large anomalies around the average climatological value of 0.08 Sv, equal for both experiments as dictated by the hydrological balance (Evaporation − Precipitation − River runoff = net flow at Gibraltar), while the outward and the inward climatological transports separately change by less than 10%, from 0.69 Sv to 0.64 Sv and from −0.61 Sv to −0.56 Sv when tidal forcing is included. Nevertheless, the larger variability of the net inflow causes the overall hydrological balance to be fulfilled only over sufficiently long timescales, while in ExpNT it holds at every time step, possibly triggering non-linear responses in the basin interior and consequently affecting its circulation. We are aware that the decrease in the outward and inward climatological transports is in contrast with the numerical results of Sannino et al. (2004), and with common knowledge of the strait dynamics. The reason for such behaviour is to be sought in a slight phase mismatch between the incoming Atlantic tide and the local equilibrium tide. As a matter of fact, phase matching is a critical requirement for a correct representation of the cumulative tidal effects of either origin, and a delicate matter of fine tuning as to its numerical prescription, the Atlantic propagating tide being imposed as a boundary condition in terms of its barotropic velocity, and not as a direct restoring term. Moreover, also the amplitude pre-scribed in the Atlantic box may be affected by errors, due to its being derived from global tidal models that already account for both effects, making it difficult to isolate the equilibrium condition needed here. Previous solutions to the problem were facilitated by the limited number of grid points which required phase tuning and by the barotropic approach (Tsimplis et al., 1995), whereas high resolution and baroclinity constitute additional difficulties in our case. A wholly satisfactory solution is still to be achieved, and its design will be the object of future research.

The basin circulation is also potentially vulnerable to the alteration of both the mean value and variability timescales of the inflowing water characteristics when tidal forcing is considered.

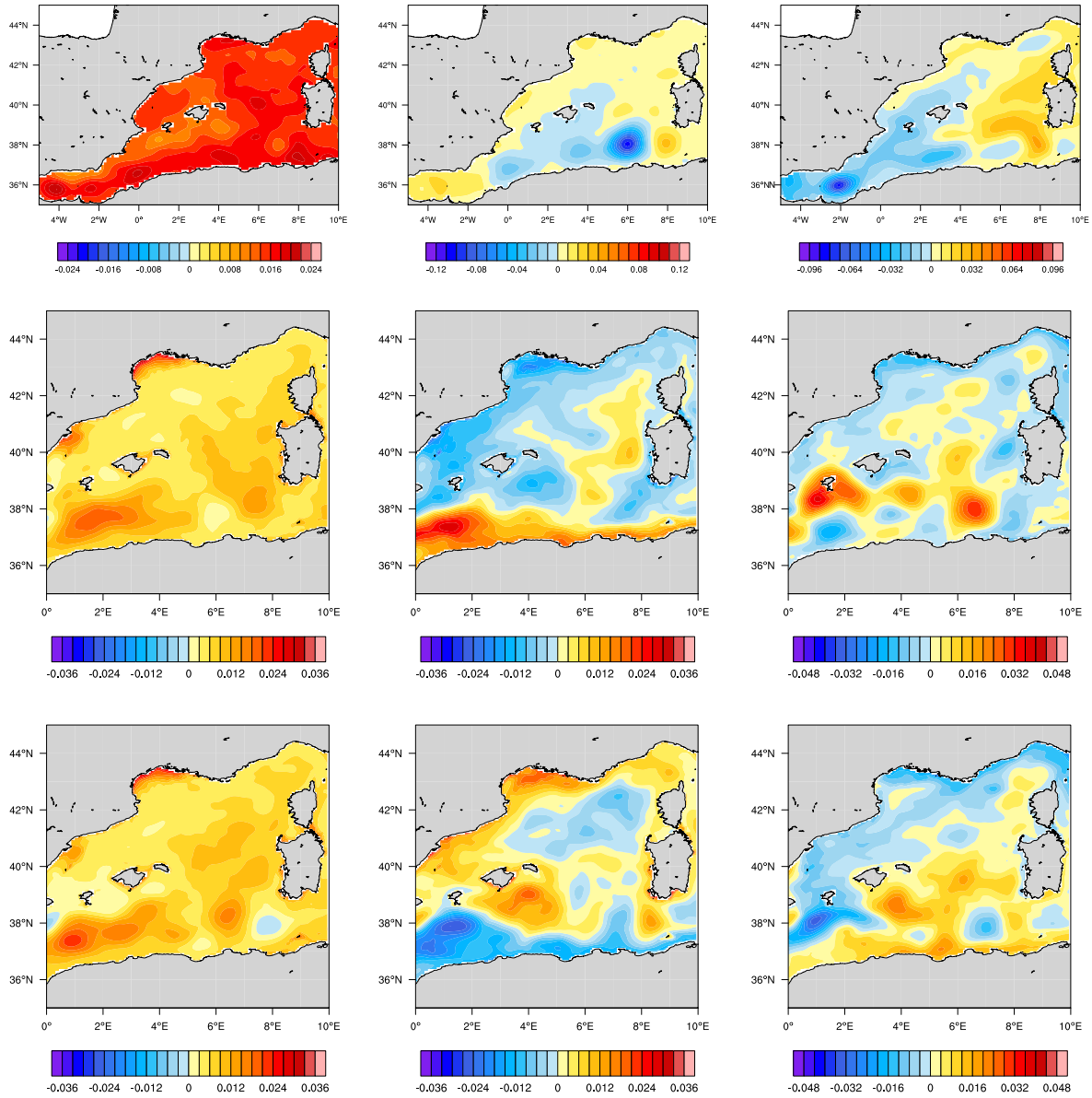

Fig. 17. First three EOF for sea level anomaly derived by AVISO (upper panel) and for temperature (vertically averaged over the upper 150 m) for ExpT (middle panel) and for ExpNT (lower panel). Explained variance is 35%, 5% and 4.6% for the three AVISO modes, 37%, 12% and 7% for ExpT and 37%, 11% and 6% for ExpNT.

Figs. 9 and 10 show salinity and temperature climatological along strait means for ExpT and ExpNT (panel a and b), as a function of longitude and depth, together with the correspondent differences between ExpT and ExpNT (panel c). As expected, the effect of tide induced mixing is to increase salinity and decrease temperature in the upper layer, the reverse occurring in the underlying water, thus giving rise to a thicker interfacial layer with respect to ExpNT. This is particularly evident just east of CS, while west of the sill the hydraulic jump itself activates strong vertical mixing also in ExpNT. These results confirm those presented in Sannino et al.(2004), obtained with a high resolution model of the SoG forced by climatological lateral boundary conditions. When tide was prescribed, they documented a maximum increase of 0.6 psu in the upper Atlantic layer due to the entrainment of Mediterranean water east of CS, and a parallel maximum decrease of 0.3 psu in the lower Mediterranean layer. The location and magnitude of enhanced mixing is shown in Fig. 11, where differences between ExpT and ExpNT are plotted. Besides the expected increase at the interface, the figure also highlights substantial effects in the bottom layer, both east and west of CS. In order to give a picture of the horizontal pattern of the variation over the area of the strait, vertical maxima were computed and plotted in Fig. 11. It is evident that in ExpT, in addition to the more significant differences inside the strait, mixing processes were also intensified in the bulk of the plume exiting the eastern mouth.

As anticipated, the presence of substantial entrainment and mixing in the strait affects the properties of the dense Mediterranean outflow, as documented by experimental data collected at the Camarinal and Espartell (ES in the following) sills. Samples of near-bottom water from the two locations were, in fact, compared, focusing in particular on the differences in extreme daily values of salinity and temperature. Bottom water was found to be around 0.1 psu saltier and 0.1 °C colder at CS than at ES, evi-dencing the entrainment and mixing occurring in the Tangier basin as the MW travels westward from CS to ES. Observations also sup-port the large time variability detected in the numerical results (García-Lafuente et al., 2007; Sanchez-Roman et al., 2009; Garcia-Lafuente et al., 2011). An analogous analysis was applied to the projected salinity and temperature time series from ExpT and ExpNT. Figs. 12 and 13 show the local series of salinity daily maxi-mum and temperature daily minimum, derived from the correspondent three-hourly series, at the two sills. The increased time variability in ExpT is evident for both variables, especially at CS where tide effects are larger. Despite the apparent noise and the moderate changes in climatological values, it is possible to extract consistent time series of salinity and temperature

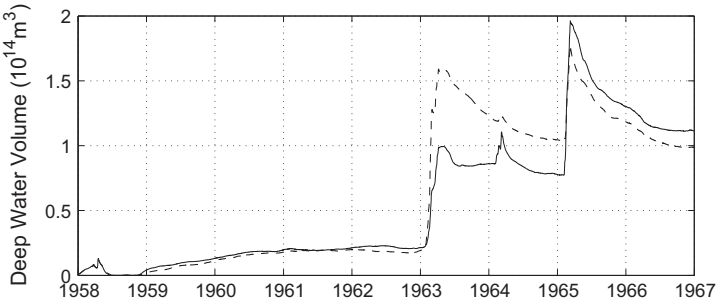

Fig. 18. Total deep water volume ($\rho > 29.10$ kg m^{-3}) stored in the Gulf of Lion area. Comparison of the ExpT (solid line) and ExpNT (dashed line). Units of 10^{14} m^3.

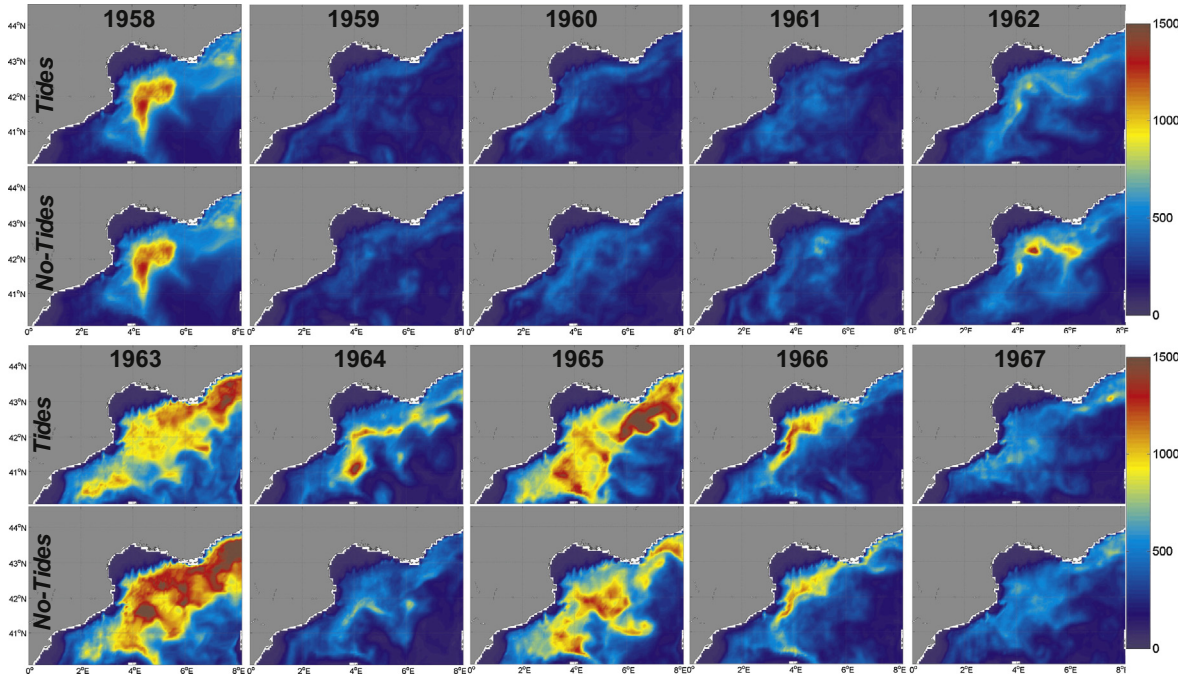

Fig. 19. Mixed layer depth time-averaged over the period January–April.

differences between the two locations, by applying a low-pass filter with a cutoff frequency of 30 days. Results are shown in Fig. 14. There is a clear indication of the enhanced mixing in ExpT, resulting in a more marked decrease in salinity along the direction of the flow, the average difference between the two locations being 0.06 psu, twice that of ExpNT, and reaching almost 0.1 psu in win-ter. Comparison of the two experiments as to the local climatological temperatures leads to similar conclusions, as in ExpT water appears to be on average 0.08 °C warmer at ES than at CS, again twice the change predicted in ExpNT, with occasional rises of more than 0.1 °C in winter. Extreme events are coherent in the two series. The reason for such agreement is that the analyzed bottom water is a sample of the Western Mediterranean Deep Water (WMDW), likely sucked at the eastern outlet of the

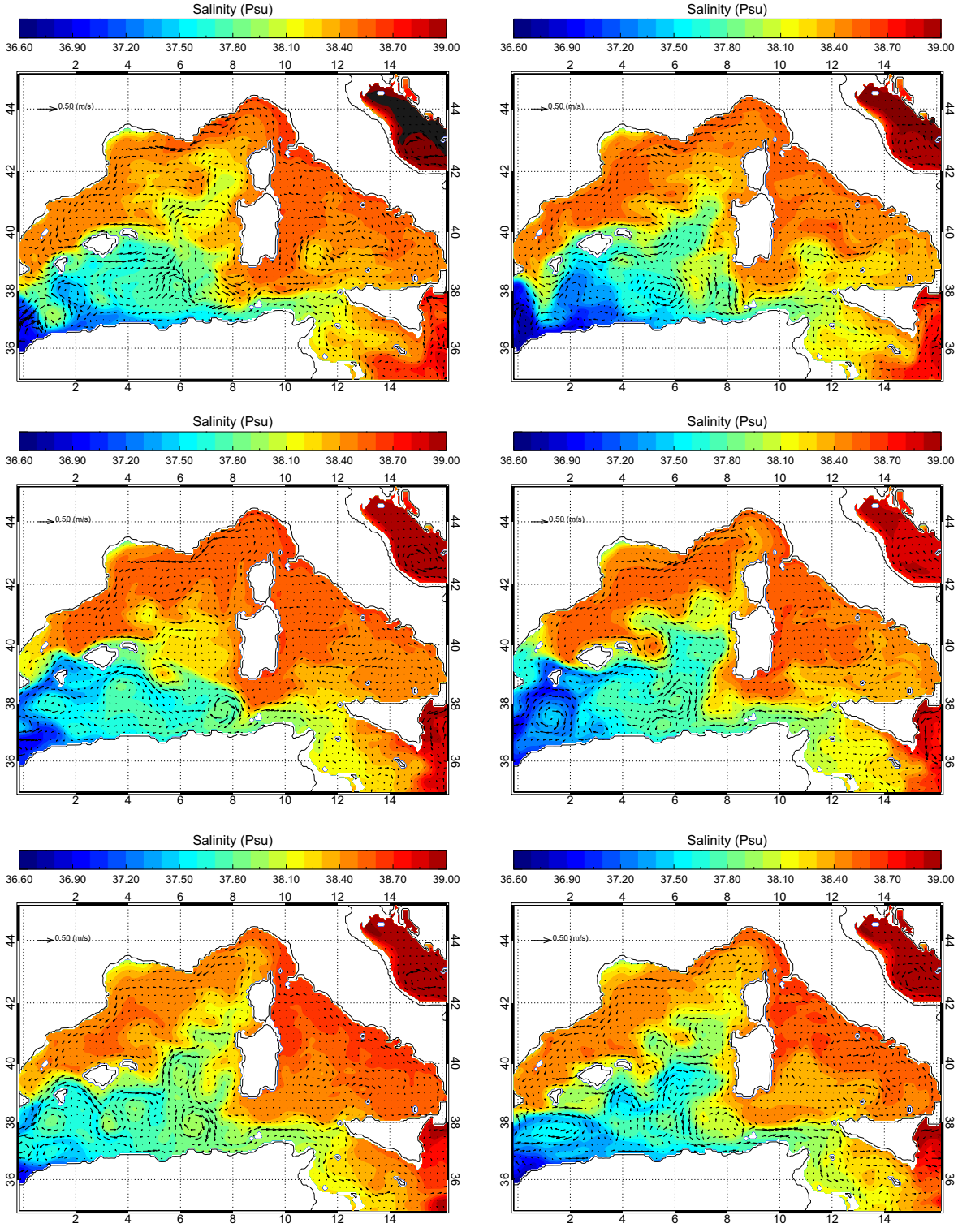

Fig. 20. Salinity at 50 m time-averaged over the period October–December 1962 (upper panel) October–December 1963 (middle panel), and October–December 1964 (lower panel). One of three values of velocity are plotted. Left ExpT, right ExpNT.

Gibraltar Strait by a Bernoulli effect (Kinder and Parrilla, 1987), whose properties are therefore unaffected by tide and well represented by the MITgcm. However, comparison of the two simulation showed that such mechanisms is more efficient when tidal forcing is included, as shown in Naranjo et al. (2014).

4.2. Basin-wide effects of tidal forcing prescription

The projected climatological temperature and salinity contents from both ExpT and ExpNT have been compared to the observations covering the simulated period contained in the MEDAR/

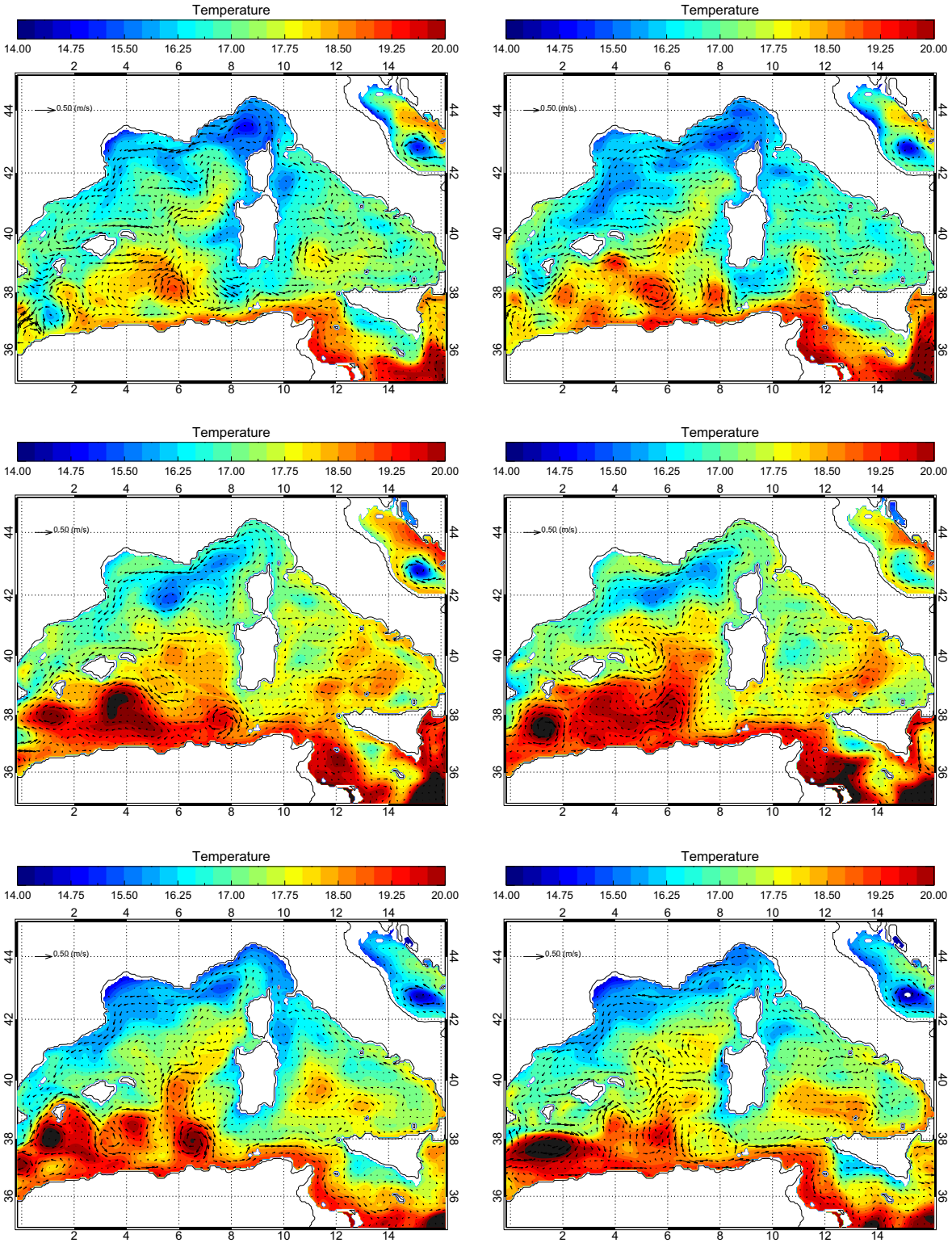

Fig. 21. Temperature at 50 m time-averaged over the period October–December 1962 (upper panel) October–December 1963 (middle panel), and October–December 1964 (lower panel). One of three values of velocity are plotted. Left ExpT, right ExpNT.

MEDATLAS-II database, which embraces years 1945–2002 and provides annual regularly gridded fields at 0.2 horizontal resolution and over 25 vertical levels, obtained by interpolating measured temperature and salinity profiles via a Variational Inverse Model (MEDAR Group, 2002). Water properties were volume averaged over the whole Mediterranean basin and then separately over its three main sub-basins (see Fig. 1), in each case alternatively integrating over the whole column or over three distinct layers covering different depths, from the surface to 100 m, from 100 m to 600 m and from 600 m to the bottom, following Rixen et al.(2005).

Results are shown in Tables 3 and 4, together with the associated standard deviation, computed from the yearly means. No error is reported for the observations as the one provided in the database is mainly attributable to data availability rather than to temporal variability (Rixen et al., 2005). Average temperatures and their variability are very similar between the two simulations, the largest differences being confined to the first 600 m in the Adriatic basin, which are warmer in ExpT. When compared to observations, however, both simulations exhibit a slight over-estimation of the global temperature, solely attributable to the deepest layers of the Eastern Mediterranean, as the other water masses are all characterized by cold biases. Again, the shallow Adriatic basin appears to host the largest discrepancies. As to salin-ity, it is generally overestimated both in ExpT and ExpNT, with maximum biases in the surface layers of the Adriatic Sea, leading to a poor representation of the local vertical gradients.

Nevertheless, the contribution to the global integral of the Adriatic being small, the reported global overestimation is mainly due to the more weighty eastern basin, also in view of the good agreement with the observations found for the western basin in both experiments. The latter, however, is the result of compensating biases along the water column, the fresher deeper layers balancing the saltier surface ones, more substantially so in ExpT.

The time evolution of the global T and S for surface, sub-surface, intermediate and deep layers is presented in Fig. 15 for both experiments. The fast responding upper layers clearly overcome the initial spin-up phase, while deeper layers still need to adjust to equilibrium, therefore suggesting to limit any further analysis to features that can be associated to faster basin reactions. However, the inclusion of tidal forcing does not affect the overall model behaviour in either experiment.

Tidal forcing effects can also be tracked in the representation of the Mediterranean average dynamics. Fig. 16 shows the climatological barotropic velocity field obtained in ExpT by averaging the 3D velocity field over depth and time. It is evident that the addition of tidal forcing does not impair the correct representation of the overall Mediterranean circulation, with the Alboran gyre still evident, as well as the two gyres in the Adriatic Sea. The comparison of ExpNT and ExpT highlights basin-wide differences of about 1 cm/s, with maxima west of Sardinia and Corsica, in the Ionian Sea, in the Southern Adriatic Sea, in the Crete-Cyprus area, and along the Moroccan coast (figure not shown). Whereas the latter can be interpreted as tide-induced residual currents, the broader

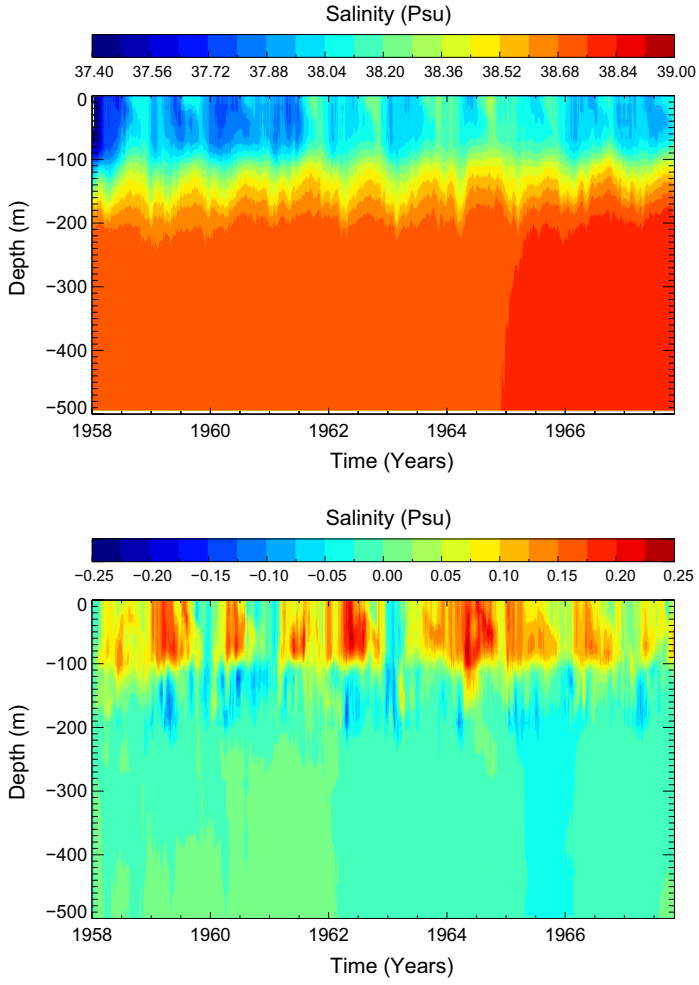

Fig. 22. Temporal evolution of salinity from ExpT (upper panel) and difference between ExpT and ExpNT (lower panel). Data are averaged over a section along the Strait of Sicily.

discrepancies appearing as organized structures, they reinforce the hypothesis of a non-negligible effect of tide prescription on the simulated mean circulation over sufficiently long time scales, when the altered characteristics of the inflow at Gibraltar and the local direct effects of tidal forcing itself will have become appreciable. Indeed, even if localized, the response to tidal forcing in the major straits (i.e. Sicily, Otranto, Balearic Sea Straits, Cretan Arc Straits and Corsica) may prove anyway crucial, as it has long been recognized that these dictate the characteristics of the network of inter-connected sub-basins that constitute the Mediterranean Sea, in terms of both allowed transports and water properties (Astraldi et al., 1999). Being the simulation too short to follow the full cycle of water masses transformation in the larger Mediterranean cell, from the inflow at Gibraltar to the spreading

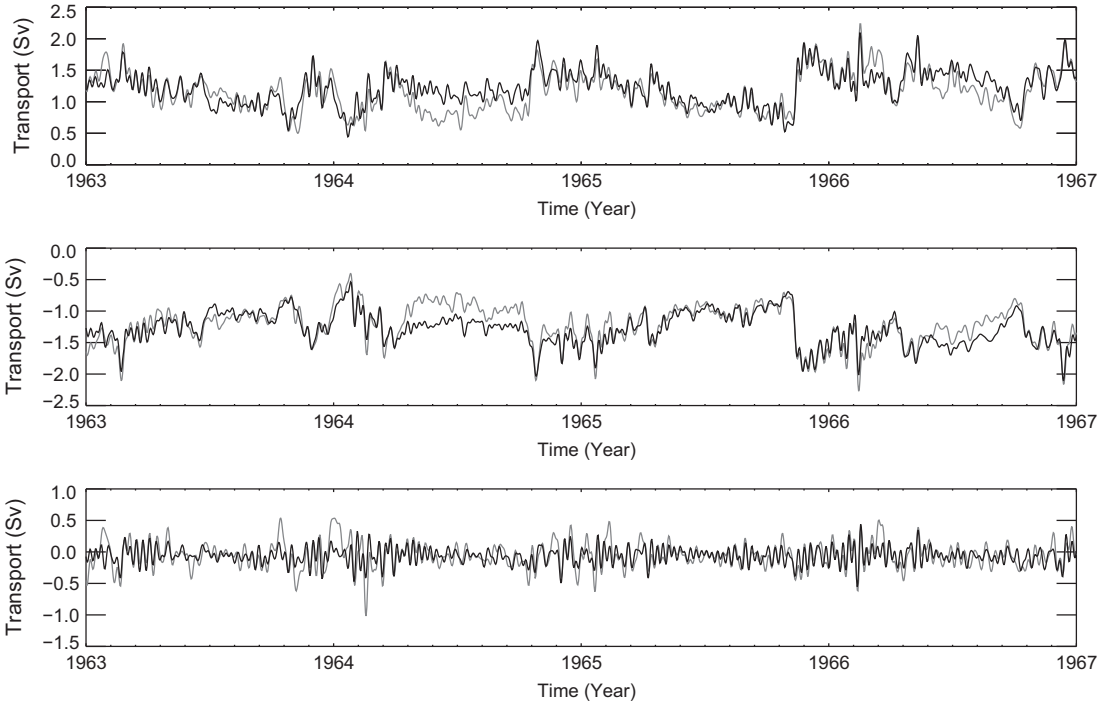

Fig. 23. Eastward (upper panel), westward (middle panel) and net (lower panel) water transports across the Sicily Strait for ExpT (grey line) and ExpNT (black line) simulations. Data have been filtered off periods less than 8 days.

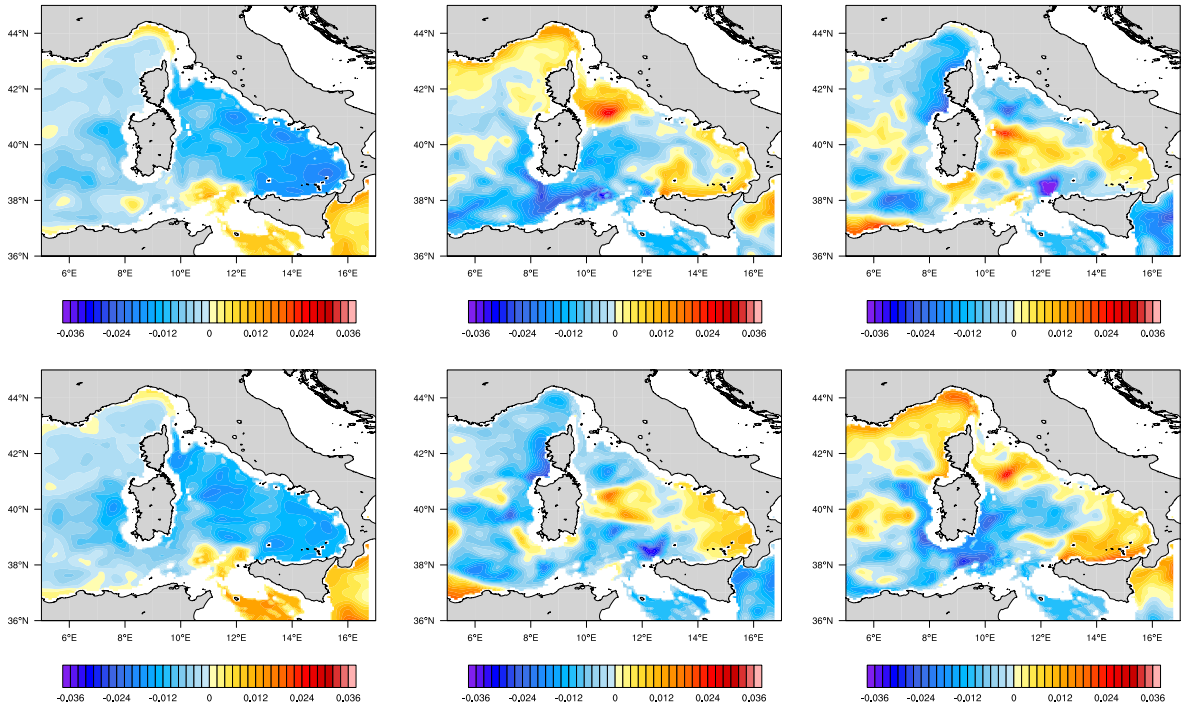

Fig. 24. First three EOFs of salinity computed over the ASO period for ExpT (upper panel) and ExpNT (lower panel. Explained variance is 58%, 11% and 8% for the three modes of ExpT, 53%, 12% and 9% for ExpNT). Data are averaged over the LIW layer.

into the Levantine basin, deep water formation, recirculation and final outflow into the Atlantic Ocean, in the following we will mainly focus on the principal features of the western basin surface circulation, tracking the signal propagating from Gibraltar along its eastward path as far as its temporary outreach, and limiting the analysis of effects in the eastern basin to the local direct responses to tidal forcing and possible interactions triggered by the altered characteristic of the upcoming Modified Atlantic Water (MAW), which were shown to be already active in the forgoing comparison.

4.2.1. MAW circulation in the western basin

East of the SoG, the inflowing Atlantic water exhibits a series of clockwise gyres and then proceeds along the Algerian Coast, mainly constrained by the Coriolis effect. Medium to large-scale instabilities arising in this current can cause Atlantic water to spread seaward as north as the Balearic Islands, and, as they travel downstream, to be trapped west of Sardinia by the local bathymetry, giving birth to a complex system of long-lived interacting open-sea eddies, which can effectively deflect the path of their mother current, both entraining it and partly letting it flow along the western coast of Corsica as an unstable vein. An ideal line connecting the Balearic Islands to the North of Corsica approximately individuates the North Balearic front that separates this recently MAW from the Northern current that re-circulates eastward along-coast after the confluence of the west-Corsica vein and of the Tyrrhenian vein upcoming through the Channel of Corsica. The latter is originated by the bifurcation of the Algerian current, which is only partly conveyed into the eastern basin thorough the Channel of Sicily (Sicilian vein), as the so-called Tunisian vein veers northward due to both topographic and steric effects (Millot and Taupier-Letage, 2005 and references therein).

We tested the hypothesis that in ExpT the altered characteristics of the inflowing Atlantic water have a non-negligible impact on the surface circulation in the western basin, by influencing the processes occurring within the accumulation area of eddies in the Western Algerian, their variability and the resulting paths of the Modified Atlantic water, with possible repercussions on the winter convection events that lead to deep water formation in the Gulf of Lions. To this end, we applied the EOF analysis to the deseasonalized sub-surface fields of temperature and salinity from both ExpT and ExpNT. Results were compared to those obtained for satellite altimetry data downloaded from AVISO (2011), which serve as a reasonable proxy for the mixed layer temperature, being the altimetric height and the temperature dependent steric height generally highly correlated (White and Tai, 1995; Willis et al., 2003). The analysis of altimetry data being constrained by data availability, it extends over a different period than that covered by the numerical experiments, but of com-parable length for the sake of climatological consistence. The first three EOFs of the 10-day averaged remotely sensed sea level anom-aly field (Fig. 17) highlight the permanent dynamic features of the western basin: the succession of gyres originated by instabilities in the Algerian current, the geographic limit of the northward disper-sal of the inflowing Atlantic water, and the coastal northern cur-rent re-circulating westward towards Gibraltar. The inherent characteristics of remotely sensed SLA fields cause all these features to be smoothed, so that the fine scale spatial variability of the basin is poorly represented. However, we expect the large scale patterns to be at least qualitatively detectable in the analogous decomposition of the modelled subsurface temperature fields, for both ExpT and ExpNT (Fig. 17). Figures are only relative to the second half of the simulations (years 1962–1967), as analyses of the first five years clearly indicated that a relatively long spin up phase had to be discarded. Despite a general resemblance of the main mode of variability in all three realizations, the spatial correlation patterns of the meandering Algerian current significantly differ between ExpT, ExpNT and the remote sensed SLA, the latter presumably giving an oversimplified description of it in terms of four stable gyres which represent a small fraction of the overall variance, with the components of the easternmost dipole alternatively in phase with either the incoming Atlantic water or with the waters dispersed towards the North. On the contrary, both numerical experiments give a more complex picture of the current, whose modes of variability substantially contribute to define also

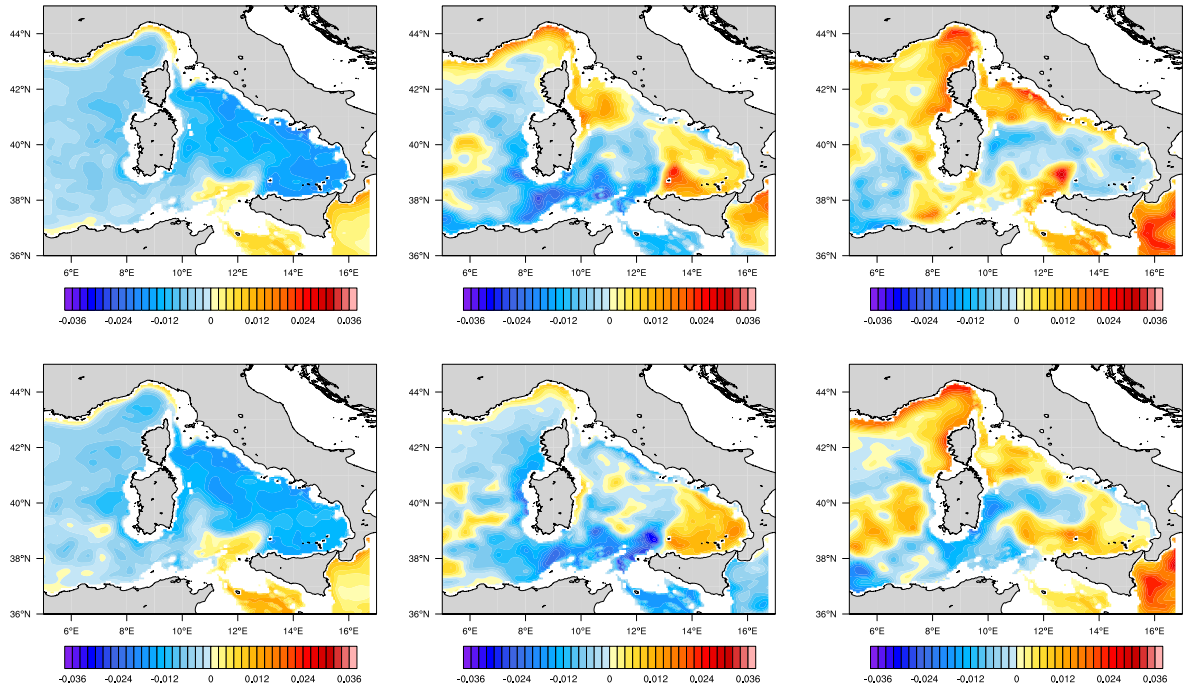

Fig. 25. First three EOFs of salinity computed over the JFM period for ExpT (upper panel) and ExpNT (lower panel). Explained variance is 53%, 11% and 8% for the three modes of ExpT, and 46%, 12% and 10% for ExpNT. Data are averaged over the LIW layer.

the first, more representative EOF, and retain considerable weight also in the second and third component. The succession of gyres is less definite, also in view of their statistical relevance being distributed among the three modes. For ExpT, in particular, in the third EOF the two westernmost gyres assume the form of dipole structures. Quite notably, the Balearic Isles, which in the SLA decomposition are apparently only subject to the northward dispersal of the incoming Atlantic water, in both experiments represent a transition zone, affected by both the competing inflow and the northern current. At the same time, the variability exhibited by the eddy accumulation basin west of Sardinia leads to the conclusion that the northward paths followed by the Modified Atlantic Water can take a variety of different directions, a feature that the SLA analysis completely fails to capture, as well as with the Balearic front. The latter exhibits different variability features in the two experiments, which can affect the paths of MAW intrusions into the northern current and cause either fresher or saltier than usual water to reside in the Gulf of Lion at the onset of winter deep convection, thus altering the local deep water formation process.

Having defined the time averaged potential density of waters below 2000 m (ρ_{2000}) as the density threshold value for the operative identification of deep water, we computed deep water volumes formed in the Gulf of Lion every winter ($\rho_{2000} = 29.10$ kg m^{-3} in the Gulf of Lion). Fig. 18 shows how deep water volumes significantly change in correspondence of the three main convection events occurring over the simulated period, namely in 1963, 1964, and 1965, with ExpT producing significantly less deep water during the first event, while exhibiting a higher, though similar in shape, peak during the third, all the more substantial as it starts from lower dense water storage. It should be noted that also the second event, while only perturbing the decay of resident deep water in ExpNT, appears as a clearly detectable peak in ExpT, and is to be considered much more pronounced in the comparison. At every grid point a vertical diffusion coefficient greater than 4 cm^{-2} s^{-1} has been used to identify the Mixed Layer Depth (Hermann et al., 2008). The analysis of the mixing layer depths over the corresponding winters (Fig. 19) confirms that only the first event is stronger in ExpNT, as was already shown in Naranjo et al. (2014). The reason for such behaviour is clearly highlighted by the comparison of ExpT and ExpNT in Figs. 20 and 21, which show how in ExpT, during the autumns preceding the convective events of 1964 and 1965, the Gulf of Lion has been filled with saltier and colder water, acting as a pre-conditioner.

When extended eastward to also include the Tyrrhenian Sea (figure not shown), the EOF analysis only highlights appreciable differences as to the behaviour of the Algerian current at the entrance of the Sicily Channel, ExpT showing a better defined

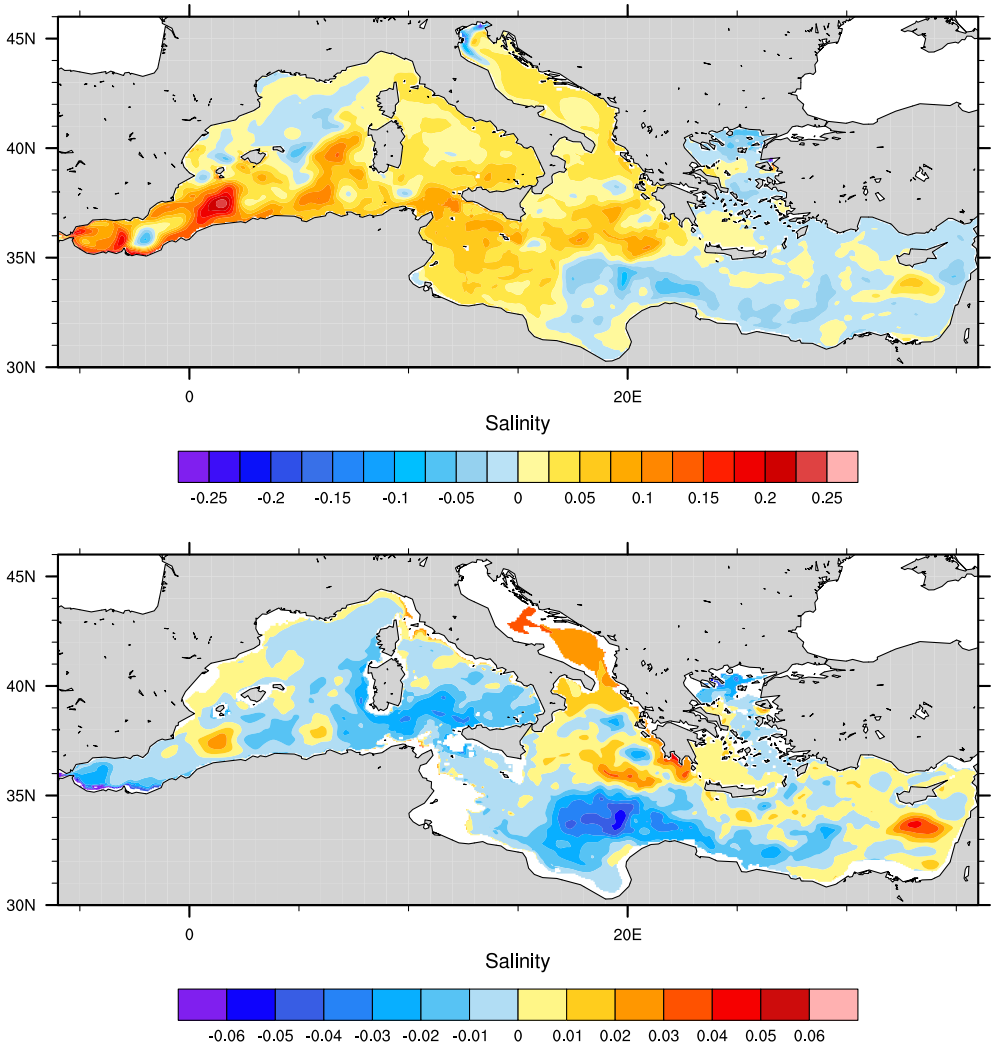

Fig. 26. Salinity difference between ExpT and ExpNT. Data are vertically averaged over the upper 150 m (upper panel) and over the layer between 150 m and 500 m (lower panel) and time-averaged over the entire simulated period.

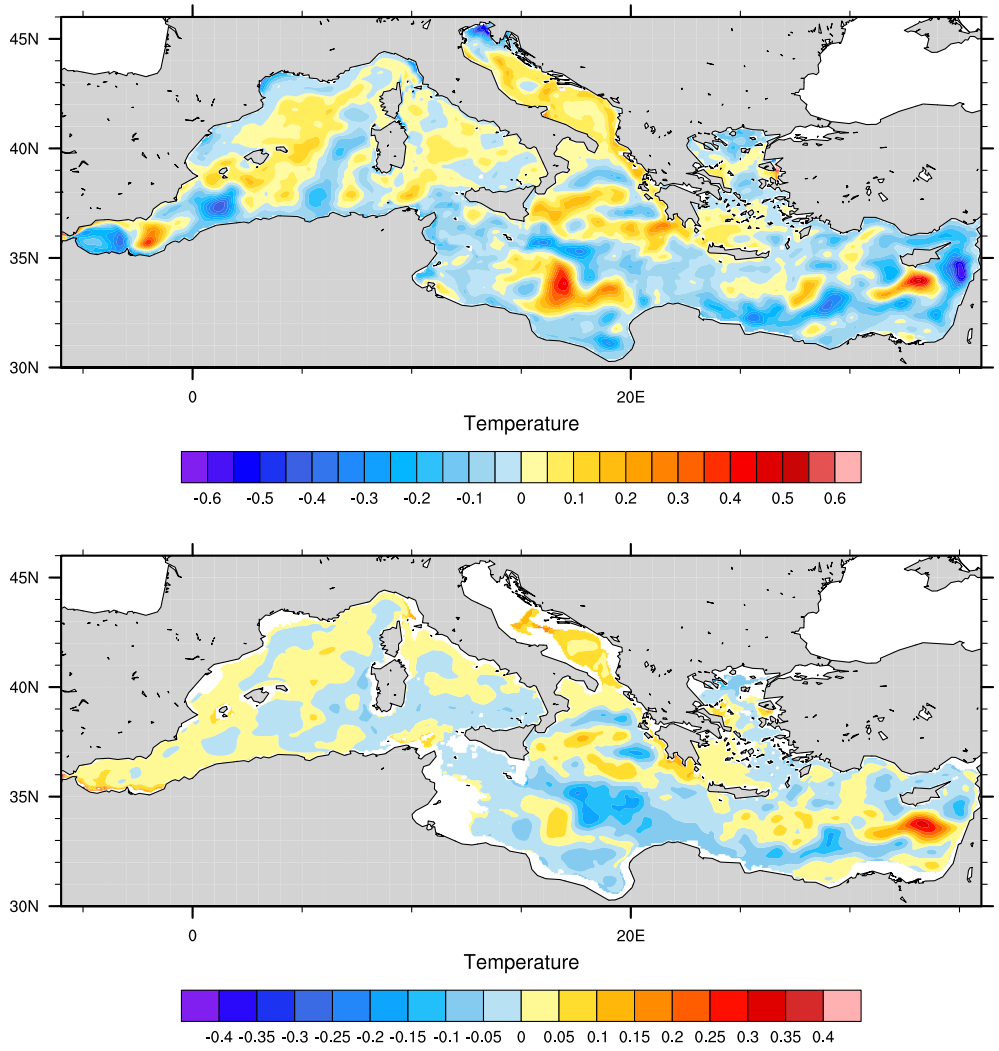

Fig. 27. Temperature difference between the ExpT and ExpNT. Data are vertically averaged over the upper 150 m (upper panel) and over the layer between 150 m and 500 m (lower panel) and time-averaged over the entire simulated period.

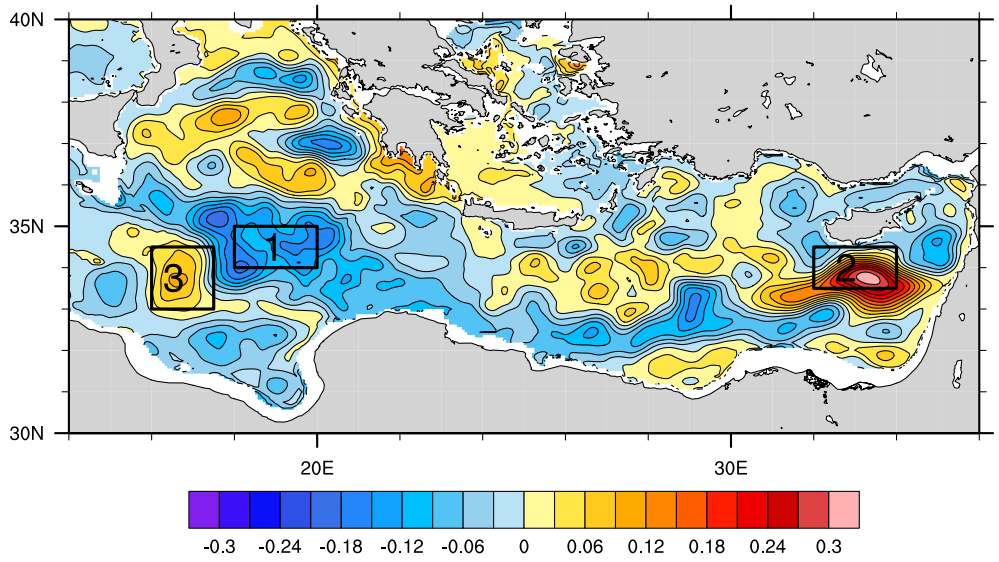

Fig. 28. Temperature difference between the ExpT and ExpNT. Data are vertically averaged between 150 m and 500 m and time-averaged over the entire simulated period. Black lines indicate areas used in Fig. 30.

stream confined along coast and sharply splitting into the two expected branches, the Sicilian and the Tunisian veins. On the contrary in ExpNT the current is occasionally allowed to spread offshore and fill the whole inlet to the channel, possibly influencing the Levantine Intermediate Water (LIW) inflow into the Tyrrhenian Sea and the Sardinia Channel.

Inside the Sicily Channel, the variability in the properties of the inflowing LIW is enhanced by the more intense vertical mixing induced by tidal forcing. Fig. 22 shows the time evolution of salinity profiles for both ExpT and ExpNT, together with the corresponding differences. The interface and surface layers appear to be affected by stronger mixing, occasionally extending to the whole water column. In terms of transports, this results in an occasionally augmented variability of the net flow, as well as in a simultaneous decrease in both the westward and eastward components which does not affect the net balance (Fig. 23). However, in addition to this direct effect LIW transport across the channel is on the long run expected to react to possible modifications arising in the eastern basin.

4.2.2. LIW circulation in the Tyrrhenian

We tested the hypothesis that also the processes governing the LIW intrusion into the western basin are sensitive to tidal forcing, by further applying our EOF analysis to the salinity fields averaged over the depth range between 300 and 600 m, where the LIW is liable to sink after passing the sill (150 m) as dictated by buoyancy constraints (Figs. 24 and 25). Current knowledge of the typical Tyrrhenian intermediate circulation identifies a few large scale, wind driven and comparatively stable cyclonic cells, mainly extending over the central and eastern part of the basin during late summer, and forming a global structure in winter, accompanied by smaller scale vortices, sometimes having surface counterparts, and acting as to divert the paths of the LIW stream (Napolitano et al., 2014). Slow transitions between this two characteristic patterns take place during spring and fall. Due to the marked seasonality of the basin circulation, the EOF analysis was separately conducted over the two stable seasons (JFM and ASO), and the examined time window consequently had to be extended to the whole simulation period for the dimension of the sample to be significant. In fact, in contrast with what was observed for the modelled MAW circulation, analysis of the underlying LIW did not require to discard a long spin-up period, the characteristics of the intermediate water inflow only being dictated by the prescribed initialization, as any transient signal carried by the newly formed water masses travelling from the east would have not reached Sicily yet. For the sake of consistency, however, we checked that the reported liability of the northern exit of the Sicily Channel to be completely filled with water of Atlantic origin is a permanent feature of ExpNT, also present during the spin-up phase. This is probably due to its being linked to the direct eastward path of the MAW stream between

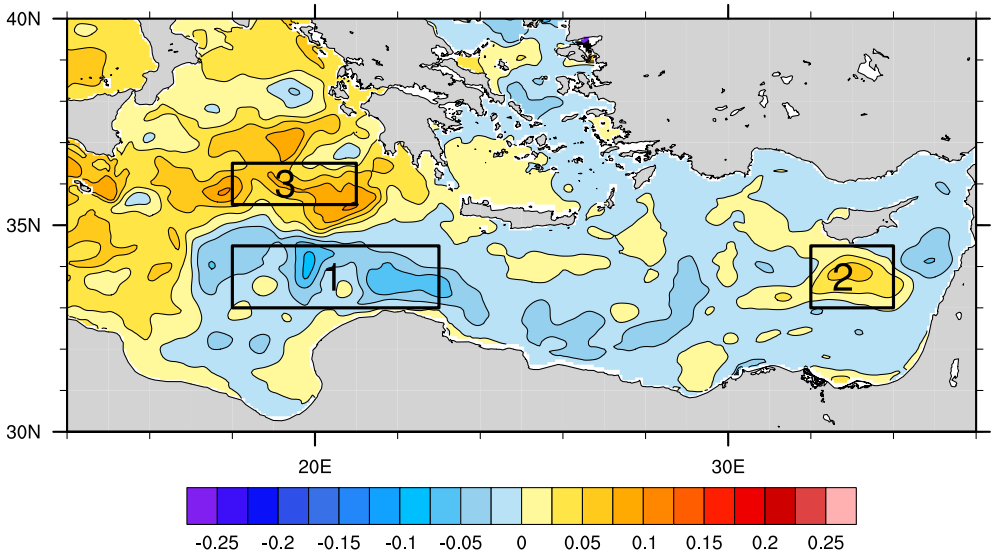

Fig. 29. Salinity difference between the ExpT and ExpNT. Data are vertically averaged over the upper 150 m and time-averaged over the entire simulated period. Black lines indicate areas used in Figs. 31.

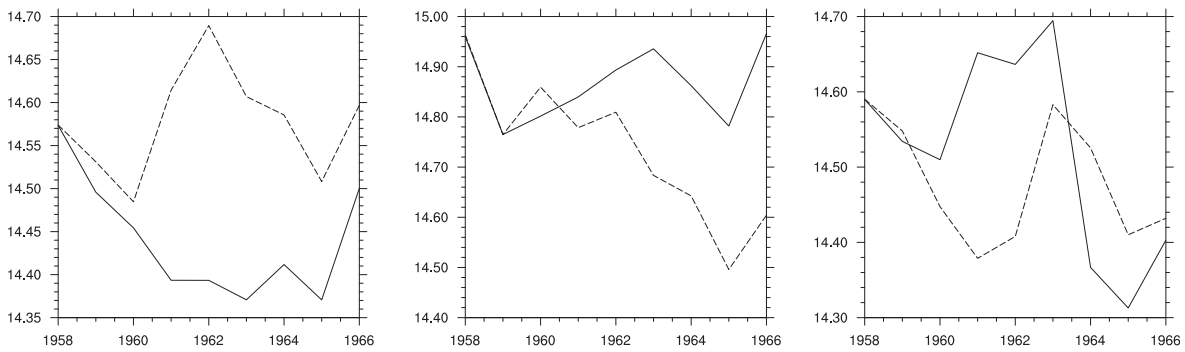

Fig. 30. Annual mean of temperature vertically averaged between 150 m and 500 m for ExpT (solid line) and for ExpNT (dashed line). Data are horizontally averaged over the areas shown in Fig. 28.

Gibraltar and Sicily (typical timescale about one year or lower), and therefore insensitive to the longer MAW re-circulation and accumulation processes occurring in the rest of the western basin. The dominant mode (first EOF) of the basin variability being mainly associated with atmospheric forcing, it displays a coherent basin-wide structure that elongates to the West to enclose the southern coast of Sardinia, and then northward along its western shores, following the paths of LIW dispersal into the Algerian basin (Millot and Taupier-Letage, 2005), and showing no correlation with the LIW crossing the Sicily Channel (figure not shown). On the contrary, both the second and third modes (Figs. 24 and 25) exhibit differences between the two experiments that appear to be related to the LIW behaviour. The dominant mode is mainly associated with the circulation of a thick (from a depth of ~300 m down to ~2000 m) layer of fluid resulting from the interaction between the inflowing LIW, water formed in the Algerian basin and resident

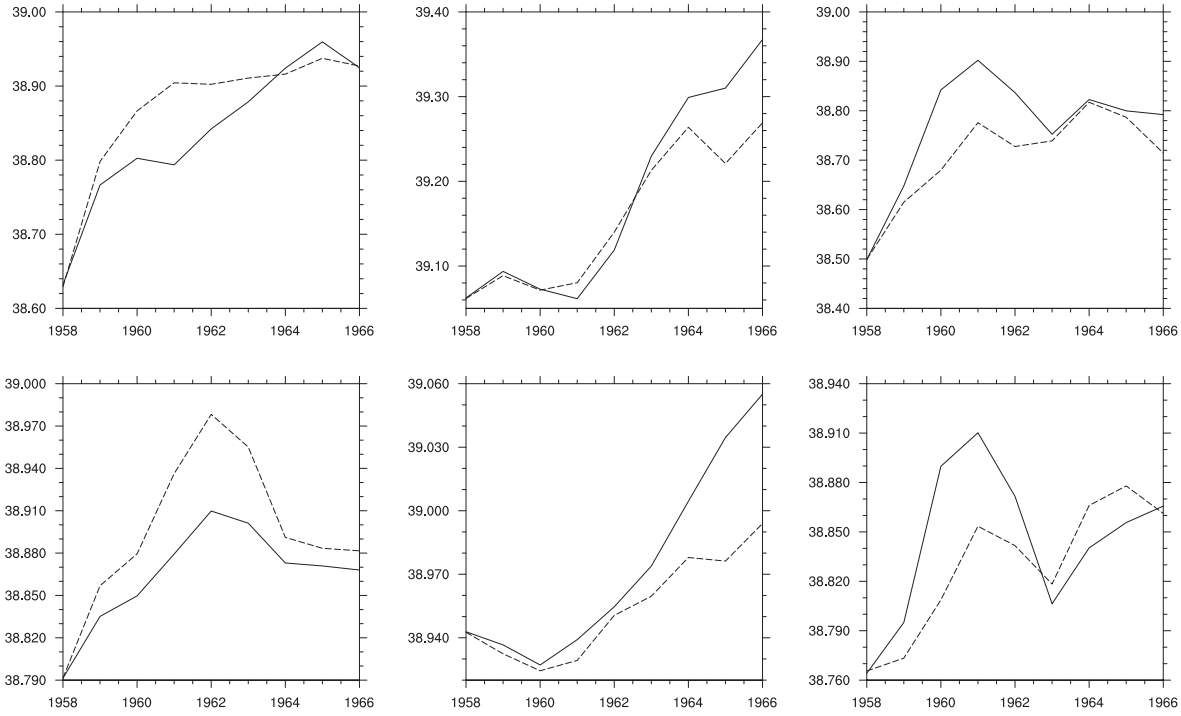

Fig. 31. Annual mean of salinity vertically averaged over the upper 150 m (upper panel) and between 150 m and 500 m (lower panel) for ExpT (solid line) and for ExpNT (dashed line). Data are horizontally averaged over the areas shown in Fig. 29.

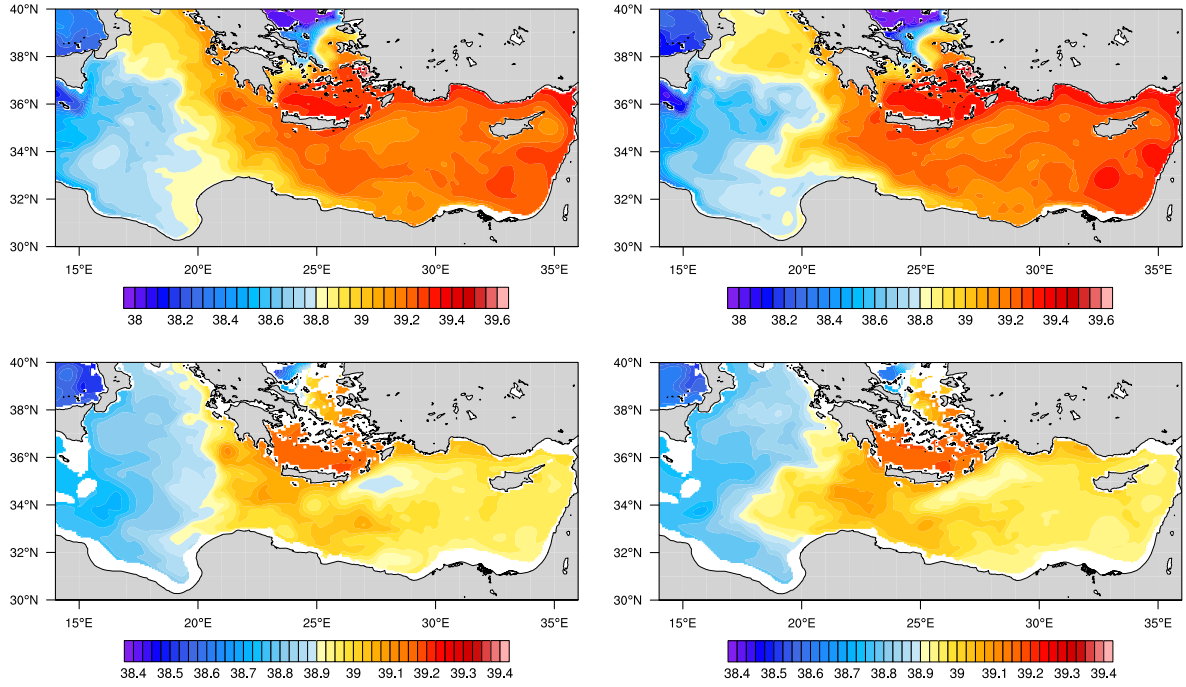

Fig. 32. Salinity time-averaged over year 1962. Upper panels refers to 30 m depth, lower panels to 400 m depth. ExpT on left panels and ExpNT on the right.

Tyrrhenian deep waters. Its structure is associated with the counter-clockwise along slope circuit that encompasses the Tyrrhenian, proceeds westward and then spreads into the Algerian Basin and northward towards the Ligurian and Provencal basins, rejoining the LIW vein that flows out of the Tyrrhenian Sea through the Channel of Corsica (Millot, 1999; Astraldi et al., 2001; Millot and Taupier-Letage, 2005). As to the seasonal differences exhibited by the second and third modes, the analysis of summer EOFs (Fig. 24) suggests that in ExpT the patterns of wind induced vari-ability which influence the LIW path on seasonal timescale are bet-ter defined, for both larger scale structures, such as the Bonifacio dipole, and finer eddies (Napolitano et al., 2014). The overall LIW course does not appear to be substantially affected, with the possible exception of more effective intrusions into the south-eastern part of the basin and of a more coherent westward stream that re-circulates along the west coast of Sardinia (second EOF of ExpT), after bordering the relatively isolated south-eastern area and delimitating a central cell bound to the north by the Bonifacio gyre (Napolitano et al., 2014). It should in fact be noted that the relative weight of the second (11%) and third (8%) modes is reversed in the two experiments, and that, while in ExpT the sec-ond EOF alone carries the signature of a well organized westward stream, the latter has been decomposed into two distinct modes in ExpNT. In ExpT the first three EOFs represent ~77% of the total variance, to be compared to the 74% of ExpNT, due to the increased statistical weight (58%) of the first mode in ExpT with respect to ExpNT (53%). The analysis of the winter modes of variability (Fig. 25) leads to similar conclusions. The first mode evidences an overall global circulation that is similar in the two experiments, although more structured in ExpT, while the second EOF of ExpT clearly highlights the presence of a smaller cyclonic cell embedded in the global one that is missing in ExpNT. It is formed by the LIW stream that exits the Sardinia Channel after meandering in the cen-tral Tyrrhenian, again limited to the North by the Bonifacio gyre (Napolitano et al., 2014), while an even more direct path to the West is exhibited by the third mode. The latter also allows tracking of the outer circuit of the LIW stream bordering the global cell and partly flowing as a vein through the Corsica Channel, and clearly evidences the reunion of the LIW paths in the Ligurian Sea. Such definite structures are missing in the ExpNT counterparts, where only the more direct path to the west is clearly depicted (now in the second EOF rather than in the third), whereas the circulation in the central Tyrrhenian appears to be blurred, just as the LIW dis-persal into the Algerian basin, and a more substantial stream of LIW apparently takes the outer northward route along the Italian coast. Such behaviour is possibly related to the reported spreading of MAW offshore the Tunisian coast and into the Tyrrhenian before entering the Sicily Channel. Again, the first mode of variability is

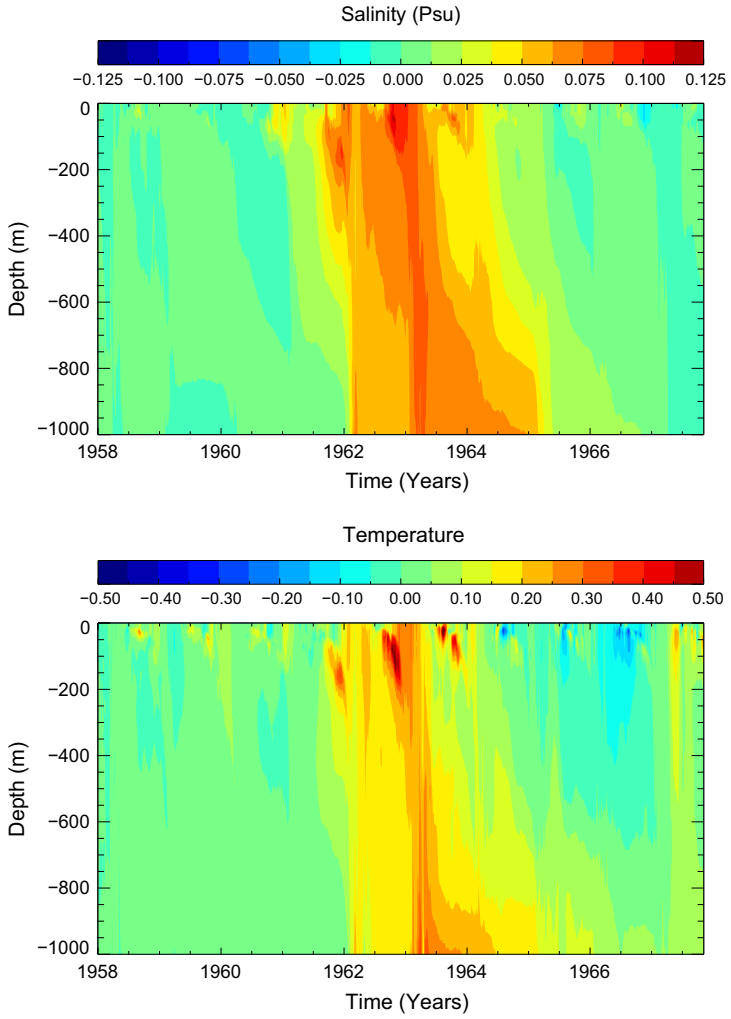

Fig. 33. Temporal evolution of the difference between ExpT and ExpNT salinity (upper panel) and temperature (lower panel). Data are averaged over the Southern Adriatic Sea.

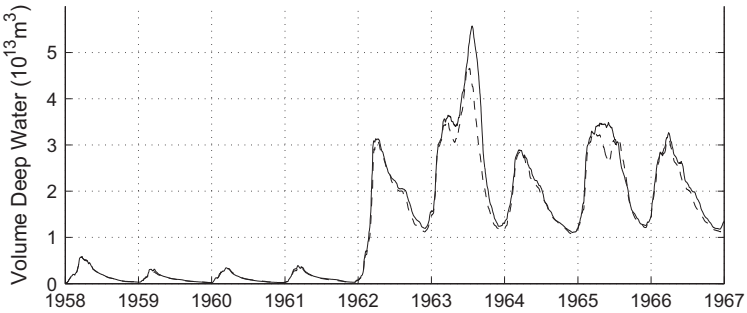

Fig. 34. Deep water volume in the Southern Adriatic convection zone, defined using a threshold for density of 29.24 kg m^3. ExpT (solid line) and ExpNT (dashed line).

reinforced in ExpT, representing 53% of the variance against the 46% of ExpNT, while the first three modes together account for 72% and 68% of the overall variability for ExpT and ExpNT respec-tively. On the whole, the inclusion of tides seems to allow a better representation of local wind driven structures, that extend well below the surface and guide the LIW paths, apparently helping transfer the stress from the surface to the underlying layers and thus homogenizing the response of a thicker layer of fluid. The reinforcement of the global cell might also be related to enhanced vertical mixing. Although these results are intrinsically qualitative and longer simulations are needed in order to assess their stability and robustness, the agreement with the results of Napolitano et al. (2014), obtained with a high resolution operative model of the Tyrrhenian, is certainly encouraging.

4.2.3. The eastern basin

Over the years, a vast literature has been dedicated to the investigation of the relative roles of the Adriatic and the Aegean Sea in acting as the main sites of deep water formation in the east-ern basin, since the Eastern Mediterranean Transient was detected by the POEM team (Roether et al., 2007). It has now long been recognized that the mechanisms which govern both the intrusion of MAW and LIW into these two marginal basins and the outflow of the newly locally formed waters, all controlled by local bathymetry, can significantly affect the dispersal paths and subsequent interactions of open sea water masses. Mixing processes induced by tidal forcing can clearly have a major influence on local mixing, and the two experiments in fact exhibit non negligible differences as to the mixing maxima in correspondence of the Cretan Arks and of the Southern Adriatic inlet (figure not shown).

However, Figures from Figs. 26 to 27 show discrepancies that are strikingly located along the path followed by the MAW in the eastern basin, and point to an indirect impact of tidal forcing as a consequence of the altered characteristics of the Atlantic inflow. Saltier water is clearly entering the Mediterranean from the SoG, filling the surface layers of the western basin and propagating eastward, as far as it is allowed by the time length of the simulation. Nevertheless, differences in the Ionian basin and further east are observed, most notably in the area encompassing Crete and Cyprus, roughly in correspondence of the Ierapetra anticyclone and of the multiple anticyclonic gyres that accumulate in the Western and Eastern Levantine basins. Such differences appear to extend down to deeper layers, whereas the large horizontally coherent structures in the Southern Ionian are essentially limited to the intermediate layers. We focused our analysis on the areas shown in Figs. 28 and 29, where the largest differences are observed for temperature and salinity, respectively. Here we computed the volume averages of potential temperature and salinity over both surface (0–150 m) and intermediate layers (150–500 m) as a function of time. The resulting relevant series are shown in Figs. 30 and 31, for the three areas in the Ionian Sea and near Cipro. It is evident that the differences in the time mean fields are originated by specific events, when the two experiments deviate from a common behaviour, namely around year 1962 for the Ionian locations, only to realigne afterwards. The same happens for the anomaly south of Rhodes, in the easternmost levantine, which is generated towards the end of the runs and has been checked to be a similarly occasional feature. For year 1962, sample surface (30 m) and intermediate (400 m) potential temperature and salinity fields are therefore shown in the panels of Fig. 32, which highlight how the saltier LIW is more effectively conveyed towards the Adriatic in ExpT, while its dispersal into the Ionian appears to be impaired. As the typical transport time of newly formed LIW from its native areas to the Ionian is esti-mated to be around 20 years (Stratford and Williams, 1997), this diversion is attributable to the clash of the costumary recirculating LIW, whose characteristics cannot have been affected by tidal forcing yet, with the upcoming altered MAW. Not surprisingly, the evolution of differences between the mean profiles of potential temperature and salinity in the Southern Adriatic Sea show positive anomalies over the same period (Fig. 33), although the magnitude of deep water volumes (ρ_{2000} = 29.24 kg m^{-3} in the Adriatic Sea) was not significantly affected due to the competing effects of temperature and salinity in determining water density (Fig. 34).

5. Conclusions

This work evaluates the effect of tidal forcing on the simulated MTHC by comparing results from two 10-year hindcast numerical simulations which also includes a high resolution representation of the SoG. The reliability of tides in the model has been preliminarly evaluated comparing amplitudes and phases derived from a barotropic version of the model against measures available in the Mediterranean basin. Sections in the SoG for the two experiments show that the enhanced mixing due to the inclusion of tide results in an increasing of salinity and a decreasing in temperature in the upper layer, the reverse occurring in the lower layer. Moreover the properties of dense water outflow between Cs and Es have been compared finding that tidal mixing determines a decrease of salinity along the strait closer to experimental data. The western basin exhibits an immediate response to the different characteristics of the inflowing AW, which is clearly depicted in the altered patterns of temperature EOFs. Deep water convection processes in the Gulf of Lion appear to be affected by such modifications, as shown by the different water volumes produced during the simulated convective events. The inclusion of tidal forcing also induces changes in the intermediate circulation of the Tyrrhenian Sea, with a better representation of local wind driven structures and a reinforcement of the global cell. LIW dispersal paths in the eastern basin are also

affected, apparently as a consequence of differences arising in the water characteristics along the eastward progress of the MAW.

Our experiments represent a first attempt to investigate the weight of tidal forcing in determining the main features of the Mediterranean thermohaline circulation, despite their being too short to fully describe both its direct impact and the mechanisms of the feedbacks it triggers within the bulk of the fluid. Longer simulations have been planned in the context of the recently approved NEMERTE project (Numerical Experiment on the Mediterranean model response to Enhanced Resolution and TidE), which was awarded 17,860,000 core hours by the Partnership for Advanced Computing in Europe (PRACE). However, even at such a preliminary stage, we can conclude that the inclusion of explicit tidal forcing in an eddy resolving Mediterranean model has non negligible effects on the simulated circulation, in addition to the expected intensification of local mixing processes. The signal induced in the MAW crossing SoG in fact propagates into the basin interior and concurs to determine the dispersal paths of the main water masses, with consequences on critical processes such as deep water formation in the Gulf of Lion and LIW recirculation.

Acknowledgements

The numerical simulation has carried out thanks to a CINECA-ISCRA HP10AB9953 type a grant. We are also grateful to the CRESCO supercomputing facilities located at ENEA (http://www.cresco.enea.it), where the model has been initially implemented and tested.

References

Adcroft, A., Campin, J.M., 2004. Rescaled height coordinates for accurate representation of free-surface flows in ocean circulation models. Ocean Modelling 7 (34), 269–284.

Adcroft, A., Hill, C., Marshall, A.J., 1997. Representation of topography by shaved cells in a height coordinate ocean model. Monthly Weather Review 125 (9), 2293–2315.

Adloff, F., Somot, S., Sevault, F., Jord, G., Aznar, R., Dqu, M., Herrmann, M., Marcos, M., Dubois, C., Padorno, E., Alvarez-Fanjul, E., Gomis, D., 2015. Mediterranean sea response to climate change in an ensemble of twenty first century scenarios. Climate Dynamics, 1–28.

Armi, L., Farmer, D.M., 1988. The flow of atlantic water through the Strait of Gibraltar. Progress in Oceanography 21, 1–105.

Astraldi, M., Balopoulos, S., Candela, J., Font, J., Gacic, M., Gasparini, G., Manca, B., Theocharis, A., Tintore, J., 1999. The role of straits and channels in understanding the characteristics of Mediterranean circulation. Progress in Oceanography 44 (1–3), 65–108.

Astraldi, M., Gasparini, G., Gervasio, L., Salusti, E., 2001. Dense water dynamics along the strait of sicily (Mediterranean sea). Journal of Physical Oceanography 31 (12), 3457–3475.

AVISO, 2011. The Altimeter Products were Produced by SSALTO/DUACS and Distributed by AVISO, with Support from CNES. <http://www.aviso.altimetry.fr/duacs/>

Bargagli, A., Carillo, A., Pisacane, G., Ruti, P.M., Struglia, M.V., Tartaglione, N., 2002. An integrated forecast system over the Mediterranean basin: extreme surge prediction in the northern adriatic sea. Monthly Weather Review 130, 1317–1332.

Bougeault, P., Lacarrere, P., 1989. Parametrization of orography-induced turbulence in a mesoscale model. Monthly Weather Review 117, 1872–1890.

Bray, N., Ochoa, J., Kinder, T.H., 1995. The role of the interface in exchange through the Strait of Gibraltar. Journal of Geophysical Research 100, 10755–10776.

Campin, J.M., Adcroft, A., Hill, C., Marshall, J., 2004. Conservation of properties in a free-surface model. Ocean Modelling 6 (34), 221–244.

Candela, J., Winant, C., Ruiz, A., 1990. Tides in the Strait of Gibraltar. Journal of Geophysical Research 95, 7313–7335.

Carillo, A., Sannino, G., Artale, V., Ruti, P.M., Calmanti, S., Dell'Aquila, A., 2012. Steric sea level rise over the Mediterranean Sea: present climate and scenario simulations. Climate Dynamics 39, 2167–2184.

Chen, C., Beardsley, R.C., 1995. A numerical study of stratified tidal rectification over finite-amplitude banks. Part i: symmetric banks. Journal of Physical Oceanography 25, 2090–2110.

Cushman-Roisin, B., Naimie, C., 2002. A 3d finite-element model of the adriatic tides. Journal of Marine Systems 37, 279–297.

Defant, A., 1961. Physical Oceanography. Pergamon Press, Oxford.

Egbert, G., Erofeeva, L., 2002. Otis – OSU tidal inversion software. <www.coas.oregonstate.edu/research/po/research/tide/otis.html>.

Farmer, D.M., Armi, L., 1988. The flow of Mediterranean water through the Strait of Gibraltar. Progress in Oceanography 21, 1–105.

Fenoglio-Marc, L., Mariotti, A., Sannino, G., Meyssignac, B., Carillo, A., Struglia, M.V., Rixen, M., 2013. Decadal variability of net water flux at the Mediterranean Sea Gibraltar Strait. Global and Planetary Change 100, 1–10.

Foreman, M.G.G., 1977. Manual for tidal heights analysis and prediction. In: Pacific Marine Sci. Rep. 77–10, 97pp.

García-Lafuente, J., 1986. Variabilidad del nivel del mar en el estrecho de gibraltar: Mareas y oscilaciones residuales. Ph.D. thesis, Inst. Esp. de Oceanogr., Fuengirola, Malaga, Spain.

García-Lafuente, J., Roman, A.S., del Río, G.D., Sannino, G., Garrido, J.S., 2007. Recent observations of seasonal variability of the Mediterranean outflow in the Strait of Gibraltar. Journal of Geophysical Research 112, C10005.

Garcia-Lafuente, J., Sanchez-Roman, A., Naranjo, C., Sánchez-Garrido, J.C., 2011. The very first transformation of the Mediterranean outflow in the Strait of Gibraltar. Journal of Geophysical Research 116 (C07010). http://dx.doi.org/10.1029/2011JC006967.

García-Lafuente, J., Pozas, E.B., Garrido, J.S., Sannino, G., Sammartino, S., 2013. The interface mixing layer and the tidal dynamics at the eastern part of the Strait of Gibraltar. Journal of Marine Systems 117-118, 31–42.

Gaspar, P., Gregoris, Y., Lefevre, J.-M., 1990. A simple eddy kinetic energy model for simulations of the oceanic vertical mixing: tests at station papa and long-term upper ocean study site. Journal of Geophysical Research 95 (C9), 16179–16193.

Hermann, M., Somot, M., Sevault, F., Estournel, C., Deque, M., 2008. Modeling the deep convection in the northwestern Mediterranean sea using an eddy-permitting and an eddy-resolving model: case study of winter 1986–1987. Journal of Geophysical Research 113 (C04011).

Janzen, C., Wong, K., 2002. Wind-forced dynamics at the estuary-shelf interface of a large coastal plain estuary. Journal of Geophysical Research, 107.

Kinder, T., Parrilla, G., 1987. Yes, some of the Mediterranean outflow does come from great depth. Journal of Geophysical Research 92, 2901–2906.

Kowalik, Z., Proshutinsky, A., 1994. The arctic ocean tides. In: Johannessen, O.M., Muench, R.D., Overland, J.E., (Eds.), The Polar Oceans and their Role in Shaping the Global Environment. Geophys. Monogr. Ser., vol. 85, pp. 137–158.

Levitus, S., 1982. Climatological Atlas of the World Ocean. NOAA Professional Paper 13, U.S. Government Printing Office, Washington, DC.

Loder, J., 1980. Topographic rectification of tidal currents on the sides of Georges Bank. Journal of Physical Oceanography 10, 1399–1416.

Loder, J., Wright, D., 1985. Tidal rectification and frontal circulation on the sides of Georges Bank. Journal of Marine Research 43 (3), 581–604.

Maas, L., Zimmerman, J., 1981. Tidal vorticity and residual circulation. Deep Sea Research 28, 195–212.

Maas, L., Zimmerman, J., 1989a. Tide-topography interaction in a stratified shelf area. i. Basic equations for quasi-nonlinear internal tides. Geophysical and Astrophysical Fluid Dynamics 45 (1–2), 1–35.

Maas, L., Zimmerman, J., 1989b. Tide-topography interaction in a stratified shelf area. ii. Bottom trapped internal tides and baroclinic residual currents. Geophysical and Astrophysical Fluid Dynamics 45 (1–2), 37–69.

Maas, L.R.M., Zimmermann, J.T.F., 1989. Tide topography interactions in a stratified shelf sea ii. bottom trapped internal tides and baroclinic residual currents. Geophysical and Astrophysical Fluid Dynamics 45 (1–2), 37–69.

Macdonald, A., Candela, J., Bryden, H., 1994. An estimate of the net heat transport through the Strait of Gibraltar. In: La Violette, P.E. (Ed.), Seasonal and Interannual Variability of the Western Mediterranean Sea. Coastal Estuarine Studies, Amer. Geophys. Union, vol. 46, pp. 13–32.

Marshall, J., Adcroft, A., Hill, C., Perelman, L., Heisey, C., 1997a. A finite-volume, incompressible Navier Stokes model for, studies of the ocean on parallel computers. Journal of Geophysical Research 102 (C3), 5753–5766.

Marshall, J., Hill, C., Perelman, L., Adcroft, A., 1997b. Hydrostatic, quasi-hydrostatic, and nonhydrostatic ocean modeling. Journal of Geophysical Research 102 (C3), 5733–5752.

MEDAR Group, 2002. Medatlas/2002 database. Mediterranean and Black Sea Database of Temperature Salinity and Bio-Chemical Parameters. Climatological Atlas. IFREMER Edition.

Millot, C., 1999. Circulation in the western Mediterranean sea. Journal of Marine Systems 20, 423–442.

Millot, C., Taupier-Letage, I., 2005. Circulation in the Mediterranean sea. In: The Mediterranean Sea. Springer-Verlag, Berlin Heidelberg, pp. 29–66. Napolitano, E., Iacono, R., Marullo, S., 2014. The 2009 surface and intermediate circulation of the tyrrhenian sea as assessed by an operational model. In: The Mediterranean Sea: Temporal Variability and Spatial Patterns. John Wiley & Sons Inc, pp. 59–74.

Naranjo, C., Garcia-Lafuente, J., Sannino, G., Sanchez-Garrido, J., 2014. How much do tides affect the circulation of the Mediterranean sea? From local processes in the Strait of Gibraltar to basin-scale effects. Progress in Oceanography 127, 108–116.

Parry, M., Canziani, O., Palutikof, J., van der Linden, P., Hanson, C. (Eds.), 2007. IPCC 2007 Fifth Assessment Report: Climate Change 2007 (AR4) Working Group II Report Impacts, Adaptation and Vulnerability. Cambridge University Press, Cambridge, United Kingdom and New York, NY, USA.

Pawlowicz, R., Beardsley, B., Lentz, S., 2002. Classical tidal harmonic analysis including error estimates in matlab using ttide. Computer and Geosciences 28, 929–937.

Rixen, M., Beckers, J.-M., Levitus, S., Antonov, J., Boyer, T., Maillard, C., Fichaud, M., Balopoulos, E., Iona, S., Dooley, H., Garcia, M.-J., Manca, B., Giorgetti, A., Manzella, G., Mikhailov, N., Pinardi, N., Zavatarelli, M., 2005. The Western

Mediterranean Deep Water: A proxy for climate change. Geophysical Research Letters 32 (L12608), 1–4.
Roether, W., Klein, B., Manca, B.B., Theocharis, A., Kioroglou, S., 2007. Transient eastern Mediterranean deep waters in response to the massive dense-water output of the aegean sea in the 1990s. Progress in Oceanography 74 (4), 540–571.
Sammari, C., Koutitonsky, V., Moussa, M., 2006. Sea level variability and tidal resonance in the gulf of Gabes, Tunisia. Continental Shelf Research 26, 338–350.
Sanchez-Garrido, J., Sannino, G., Liberti, L., Garcia Lafuente, J.L.P., 2011. Numerical modelling of three-dimensional stratified tidal flow over camarinal sill, Strait of Gibraltar. Journal of Geophysical Research 116 (C12), 1978–2012.
Sanchez-Roman, A., Sannino, G., Garcia-Lafuente, J., Carillo, A., Criado-Aldeanueva, F., 2009. Transport estimates at the western section of the Strait of Gibraltar: a combined experimental and numerical modeling study. Journal of Geophysical Research, 114.
Sannino, G., Bargagli, A., Artale, V., 2004. Numerical modeling of the semidiurnal tidal exchange through the Strait of Gibraltar. Journal of Geophysical Research 109, C05011. http://dx.doi.org/10.1029/2003JC002057.
Sannino, G., Herrmann, M., Carillo, A., Rupolo, V., Ruggiero, V., Artale, V., Heimbach, P., 2009. An eddy-permitting model of the Mediterranean sea with a two-way grid refinement at the Strait of Gibraltar. Ocean Modelling 30 (1), 56–72.
Sannino, G., Pratt, L., Carillo, A., 2009. Hydraulic criticality of the exchange flow through the Strait of Gibraltar. Journal of Physical Oceanography 39 (11), 2779–2799.
Sannino, G., Sanchez Garrido, J.C., Liberti, L., Pratt, L., 2014. Exchange flow through the Strait of Gibraltar as simulated by a-coordinate hydrostatic model and a z-coordinate nonhydrostatic model. In: The Mediterranean Sea: Temporal Variability and Spatial Patterns. John Wiley & Sons Inc, pp. 25–50.
Sanz, J.L., Acosta, J., Esteras, M., Herranz, P., Palomo, C., Sandoval, N., 1991. Prospección geofísica del Estrecho de Gibraltar: resultados del Programa Hércules (1980–1983). Publ. espec. Inst. Esp. Oceanogr. Span. Inst. of Oceanogr, Madrid.
Somot, S., Sevault, F., Deque, M., 2006. Transient climate change scenario simulation of the Mediterranean sea for the twenty-first century using a high-resolution ocean circulation model. Climate Dynamics 27 (7–8), 851–879.
Stanev, E., Traon, P.L., Peneva, E., 2000. Sea level variations and their dependency on meteorological and hydrological forcing: analysis of altimeter and surface data for the Black Sea. Journal of Geophysical Research 105 (C7), 17203–17216.
Stratford, K., Williams, R.G., 1997. A tracer study of the formation, dispersal, and renewal of levantine intermediate water. Journal of Geophysical Research 102 (C6), 12539–12549.
Struglia, M., Mariotti, A., Filograsso, A., 2004. River discharge into the Mediterranean sea: climatology and aspects of the observed variability. Journal of Climate 17, 4740–4751.
Tee, K.T., 1985. Depth-dependent studies of tidally induced residual currents on the sides of Georges Bank. Journal of Physical Oceanography 15, 1818–1846.
Thorpe, R., Bigg, G., 2000. Modelling the sensitivity of the Mediterranean outflow to anthropogenically forced climate change. Climate Dynamics, 16.
Tsimplis, M., Proctor, R., Flather, R., 1995. A two-dimensional tidal model for the Mediterranean sea. Journal of Geophysical Research 100 (C8), 16223–16239.
Vergos, G.S., Bayoud, F., Sideris, M., Tziavos, I., 2002. High-resolution geoid computation by combining shipborne and multi-satellite altimetry data in the eastern Mediterranean sea. IGeS Bulletin, 13.
Vincent, P., Canceill, P., 1993. Oceanic tides in the Mediterranean sea. International Geoid Service Bulletin 2, 84–90.
White, W.B., Tai, C.-K., 1995. Inferring interannual changes in global upper ocean heat storage from TOPEX altimetry. Journal of Geophysical Research: Oceans 100 (C12), 24943–24954. http://dx.doi.org/10.1029/95JC02332.
Willis, J.K., Roemmich, D., Cornuelle, B., 2003. Combining altimetric height with broadscale profile data to estimate steric height, heat storage, subsurface temperature, and sea-surface temperature variability. Journal of Geophysical Research: Oceans 108 (C9), 1–12. http://dx.doi.org/10.1029/2002JC001755.
Zimmerman, J., 1981. Topographical rectification: a comment on spectral representation. Journal of Physical Oceanography 11, 1037–1039.